

Single Molecule Observations of Receptor:Ligand Binding  
at Live T Cell-Supported Membrane Interfaces

By

Katherine Nell Alfieri

A dissertation submitted in partial satisfaction of the

requirements for the degree of

Doctor of Philosophy

in

Chemistry

in the

Graduate Division

of the

University of California, Berkeley

Committee in charge:

Professor Jay T. Groves, Chair  
Professor Daniel Alden Fletcher  
Professor Ke Xu

Summer 2015

Single Molecule Observations of Receptor:Ligand Binding  
at Live T Cell-Supported Membrane Interfaces

Copyright © 2015

by

Katherine Nell Alfieri

## Abstract

### Single Molecule Observations of Receptor:Ligand Binding at Live T Cell-Supported Membrane Interfaces

by

Katherine Nell Alfieri

Doctor of Philosophy in Chemistry

University of California, Berkeley

Professor Jay T. Groves, Chair

Recognition of antigen by T cells occurs at the junction between a T cell and an antigen-presenting cell. Within this highly constrained interface, the T cell receptor (TCR) interacts with its cognate antigen peptide major histocompatibility complex (pMHC). Additional signaling and adhesion molecules present in this intercellular environment influence its overall topography and geometry, which can significantly impact receptor:ligand binding events. The work presented in this dissertation describes three studies aimed at making direct, *in situ* measurements of molecular interactions during T cell signal transduction. For all of these studies, I use a hybrid live T cell-supported membrane system to mimic the physiological juxtacrine signaling environment and single molecule fluorescence microscopy to monitor individual receptor:ligand binding events. The supported membrane is functionalized with fluorescently-tagged pMHC and the formation of individual pMHC:TCR complexes is observed via time-resolved single molecule techniques. Using these approaches, I report live cell, two-dimensional pMHC:TCR kinetics and affinity measurements in self-reactive human T cell clones and discuss discrepancies between my results and those determined via mechanical assays. I also describe a novel method for simultaneously monitoring pMHC:TCR binding and downstream cellular response in a single cell. This strategy allows the measurement of all pMHC:TCR interactions leading to T cell activation and reveals a cumulative dwell time threshold required for activation. In order to better understand the molecular interactions of the costimulatory protein CD80, I have developed a novel CD80-SNAP-tag reagent suitable for single molecule receptor:ligand binding studies. I discuss the design, characterization, and application of this reagent, which has been used to demonstrate global environmental changes in the membrane-membrane interface during T cell triggering. Together, these studies emphasize the importance of investigating ligand binding in a physiologically relevant context and will contribute to a better understanding of the early stages of T cell signaling.

To my parents

# Table of Contents

<b>Chapter 1: Introduction .....</b>	<b>1</b>
Section 1.1: Signal transduction at the T cell-antigen-presenting cell interface.....	1
Section 1.2: Investigating T cell signaling using supported membranes .....	2
Section 1.3: Considerations for single molecule studies .....	3
Section 1.4: Current objectives .....	4
Section 1.5: Chapter 1 references .....	4
<b>Chapter 2: Single Molecule Measurements of pMHC:TCR Binding in Self-Reactive Human T Cells .....</b>	<b>9</b>
Section 2.1: Introduction.....	9
Section 2.2: Experimental setup .....	10
Section 2.3: Peptide and protein preparation and characterization .....	11
Section 2.4: Single molecule measurements of pMHC:TCR kinetics and affinity in self-reactive human T cell clones .....	18
Section 2.5: Discussion and conclusions .....	24
Section 2.6: Materials and methods .....	26
Section 2.7: Chapter 2 references .....	30
<b>Chapter 3: The Development of a Novel CD80 Supported Membrane Reagent for Single Molecule Investigations of T Cell Signaling .....</b>	<b>33</b>
Section 3.1: Introduction.....	33
Section 3.2: Experimental design .....	33
Section 3.3: Protein preparation and characterization .....	36
Section 3.4: Monitoring CD80 binding events during TCR triggering .....	44
Section 3.5: Discussion and conclusions .....	48
Section 3.6: Materials and methods .....	49
Section 3.7: Chapter 3 references .....	52
<b>Chapter 4: Probing pMHC:TCR Binding Thresholds for T cell Activation .....</b>	<b>57</b>
Section 4.1: Introduction.....	57
Section 4.2: Experimental design .....	58
Section 4.3: Quantification of pMHC:TCR binding events leading to cellular activation.....	61
Section 4.4: Discussion and conclusions .....	63
Section 4.5: Materials and methods .....	63
Section 4.6: Chapter 4 references .....	66

## **Acknowledgements**

I would like to acknowledge everyone who has supported me throughout my graduate career, both in Berkeley and from afar. Without a doubt, none of this would be possible without my parents' encouragement, patience, and humor. I've been lucky to have an amazing network of friends at UC Berkeley, who have made the last five years a truly fun experience. Keeping in touch with friends and loved ones outside of the scientific and academic worlds has helped me to keep everything in perspective and has given me a greater appreciation for my research. My advisor, Jay Groves, has always encouraged me when experiments weren't working and helped me step back and see the bigger picture. Finally, I must acknowledge the Groves lab, which I initially joined, not only for the science, but also for some of the most fun and friendly scientists I have ever met. The collaborative atmosphere is unparalleled and none of the work described in this dissertation would be possible without the help of Jenny Lin, Nicole Fay, Mike Coyle, Geoff O'Donoghue, and Rafal Pielak. I would especially like to acknowledge Jenny Lin, with whom much of the work described in Chapters 2 and 4 was done as part of a fruitful collaboration over the past year and a half.

# Chapter 1

## Introduction

### Section 1.1: Signal transduction at the T cell-antigen-presenting cell interface

The adaptive immune system is responsible for recognizing foreign molecules originating from pathogens and selectively eliminating the invading microorganisms. This process is initiated by helper T cells, which bind the foreign molecules, or antigens, via a cell-surface protein called the T cell receptor (TCR). T cells can only recognize antigen that is bound to major histocompatibility complex (MHC) molecules on the membrane of antigen-presenting cells (APCs). The binding of TCR to antigen-MHC activates the T cell and triggers a signaling pathway that eventually leads to the transcription and secretion of cytokines, which play an important role in activating B cells, cytotoxic T cells, macrophages, and various other cells that participate in the immune response.<sup>1</sup>

T cells are capable of discriminating between structurally similar foreign antigen peptides (non-self) and non-stimulatory self peptides with high sensitivity and selectivity.<sup>2</sup> Research has revealed that T cells respond upon recognition of as few as a single agonist peptide-MHC (pMHC)<sup>3</sup> and are able to specifically recognize one foreign pMHC in the presence of a large excess of self-pMHCs.<sup>4</sup> The basis of antigen recognition resides in subtle, peptide-specific differences in binding between pMHC and TCR.<sup>5, 6</sup> In particular, differences in the kinetic off-rates of pMHC:TCR binding have been implicated in peptide discrimination and described in the kinetic proofreading model. This model proposes that the full activation of a T cell requires the pMHC:TCR interaction to be sustained long enough to complete a series of necessary modification steps, correlating reciprocal off-rates and peptide potencies.<sup>7, 8</sup>

The ability of T cells to distinguish self from non-self and respond only to foreign antigens is integral to the successful functioning of the adaptive immune system. Failure of this recognition process results in an inappropriate response to self and can lead to the pathogenesis of autoimmune disorders. Autoimmune disease is characterized by T cell recognition of self-antigens presented by MHC molecules. T cells that recognize and respond to self, which are referred to as self-reactive T cells, are typically eliminated from the immune repertoire during a process called negative selection.<sup>1</sup> In the case of autoimmune disease, self-reactive T cells escape negative selection through an unknown mechanism. Multiple theories to explain this phenomena center around the kinetic parameters of self-pMHC:TCR binding, including low affinities due to structural

alterations<sup>9, 10, 11</sup> and fast off-rates that lie below a kinetic threshold.<sup>12, 13</sup>

Antigen recognition occurs in the context of many other key protein interactions contributing to TCR triggering.<sup>14</sup> One such interaction is between CD80 on the antigen-presenting cell and its ligand, CD28 or CTLA-4, on the T cell surface. The initial TCR signal is amplified in a process called costimulation, which is mediated by CD80:CD28 binding and is required for full T cell activation in the presence of very little antigen.<sup>15, 16</sup> In contrast, the interaction between CD80 and CTLA-4 is inhibitory and is involved in the negative regulation of T cell signal transduction.<sup>17, 18</sup> Modulation of costimulatory signals for T cell activation is a promising strategy for the treatment of autoimmune diseases, prevention of graft versus host disease in transplantation, and antitumor immunity.<sup>19</sup>

While the membrane proteins involved in T cell activation are crucial for initiating signal transduction, the membrane environment itself plays a critical role in early signaling events. T cell signaling is a type of juxtacrine signaling, which occurs at the junction between two apposing cell membranes. The binding of T cell surface receptors to their cognate APC ligands leads to cell spreading and the formation of a planar signaling interface at the area of cell-cell contact.<sup>20, 21</sup> Cell spreading and adhesion are aided by the interaction between the integrin lymphocyte function associated antigen-1 (LFA-1) on the T cell and the adhesion molecule intercellular adhesion molecule 1 (ICAM-1) on the antigen-presenting cell surface.<sup>22, 23</sup> This highly constrained intercellular environment can significantly impact the pMHC:TCR molecular binding events on which antigen discrimination is based.<sup>24, 25</sup>

## **Section 1.2: Investigating T cell signaling using supported membranes**

Progress has been made in understanding T cell activation in the context of juxtacrine signaling through the use of supported phospholipid membranes. These artificial, planar membranes are formed by spontaneous fusion of small lipid vesicles onto a hydrophilic surface such as silicon oxide and can be functionalized with cell surface ligands using bioconjugation techniques.<sup>26, 27</sup> Lipids and membrane-linked proteins in the supported lipid bilayer can diffuse freely over macroscopic distances, mimicking lateral diffusion in the two-dimensional cell membrane.<sup>28, 29</sup> For T cell signaling studies, the supported membrane replaces the antigen-presenting cell, which is reconstituted by linking pMHC and ICAM-1, at minimum, to the phospholipid head groups. This artificial membrane can be interfaced with T cells to create a hybrid T cell-supported membrane system.<sup>30</sup>

The use of the hybrid T cell-supported membrane system in investigating T cell signal transduction offers several advantages over more traditional biochemical<sup>31</sup> and cell biology<sup>32</sup> approaches. Reconstitution of the APC membrane surface allows for precise

control over the lipids and ligand proteins displayed on the surface. By tuning the chemical composition of supported membranes, we can create a range of biocompatible interfaces with controllable physical properties, such as surface density of molecules<sup>33</sup> and degree of molecular clustering.<sup>34</sup> In addition, supported membranes are compatible with micro/nano-fabrication techniques and fluorescence microscopy. Through fabrication of the solid supported membrane substrates, one can create spatially<sup>35</sup> or curvature<sup>36</sup> patterned membranes to investigate many aspects of T cell signaling.<sup>28</sup> Finally, the use of the hybrid T cell-supported membrane system permits the imaging and tracking of proteins in the intercellular junction using total internal reflection fluorescence (TIRF) microscopy, which only images fluorescent molecules at the cell-cell interface.<sup>26, 37</sup>

Supported membranes have been utilized for over thirty years<sup>26</sup> to study T cell signaling and have led to a number of critical advances in the field. The experimental platform was shown to successfully activate T cells and could be used to recreate the immunological synapse that had been observed to form between a T cell and antigen-presenting cell.<sup>30, 32</sup> The immunological synapse, a bulls-eye pattern with pMHC:TCR at the center and a ring of ICAM-1:LFA-1 at the periphery, was thought to be critical for sustained signaling. By lithographically patterning diffusion barriers onto the solid membrane support, it was demonstrated that the synapse actually downregulates TCR activation. The diffusion barriers prevented the formation of the immunological synapse, which resulted in sustained calcium signaling.<sup>35</sup> Other studies have revealed T cell triggering thresholds,<sup>38</sup> shed light on the role of the cytoskeleton in the activation process,<sup>39, 40</sup> and allowed the measurement of single molecule two-dimensional pMHC:TCR kinetics.<sup>41</sup>

### **Section 1.3: Considerations for single molecule studies**

As described previously, TCR-mediated antigen recognition requires the detection of a very weak ‘signal’ (low copy numbers of foreign antigen-MHC) in the presence of high levels of ‘noise’ (abundant self-pMHC). At physiological densities of agonist peptide, pMHC:TCR binding events are rare and difficult to detect using traditional biochemistry and cell biology assays. However, time-resolved single molecule techniques are sensitive enough to discern rare or low signal events and capture the stochastic nature of individual pMHC:TCR interactions.<sup>42</sup> Such methods can also be applied to other protein dynamics during T cell activation in order to directly measure distributions in molecular properties, which must be inferred indirectly in ensemble experiments, or to detect rare species or states, which are averaged in an ensemble.<sup>43</sup>

Due to the ability to control the protein composition and surface density of the surrogate APC membrane, the hybrid T cell-supported membrane system is ideal for single molecule studies of T cell signaling. In setting up the artificial bilayer system, care must be taken in choosing the method of fluorescent tagging, as well as the fluorophores themselves. The protein of interest should be labeled with a fluorescent probe in a 1:1

stoichiometry, such that detection of a single dye molecule corresponds to detection of a single protein monomer. In general, collecting more photons increases the signal to noise ratio and thus the precision of tracking single molecules. The use of bright, photostable fluorophores increases the precision of the measurement and allows proteins to be tracked longer.<sup>43</sup>

## Section 1.4: Current Objectives

In this dissertation, I present three studies aimed at investigating single molecule membrane receptor:ligand binding and kinetics during T cell signal transduction. In particular, I am interested in understanding key membrane surface chemical reactions in the context of the highly constrained T cell-antigen-presenting cell interface. To accomplish these goals, the work described here utilizes the supported membrane system, 1:1 bioconjugation and fluorescent tagging methods, and time-resolved single molecule fluorescence microscopy and spectroscopy techniques. In addition, traditional cell biology, molecular biology, and biochemical methods are used for the completion of this work. In Chapter 2, I discuss *in situ* measurements of two-dimensional single molecule pMHC:TCR kinetics and affinity in self-reactive human T cell clones and compare my results to those determined via mechanical assays. In Chapter 3, I describe the development, characterization, and application of a novel CD80 reagent suitable for single molecule receptor:ligand binding studies. Finally, Chapter 4 presents recent work toward establishing a pMHC:TCR binding threshold required for T cell activation.

## Section 1.5: Chapter 1 references

1. Kindt, T. J.; Osborne, B. A.; Goldsby, R. A., *Kuby Immunology*. 6 ed.; W.H. Freeman: 2007.
2. Weiss, A.; Littman, D. R., Signal transduction by lymphocyte antigen receptors. *Cell* **1994**, *76*, 263-274.
3. Irvine, D. J.; Purbhoo, M. A.; Krogsgaard, M.; Davis, M. M., Direct observation of ligand recognition by T cells. *Nature* **2002**, *419*, 845-849.
4. Huang, J.; Meyer, C.; Zhu, C., T cell antigen recognition at the cell membrane. *Molecular Immunology* **2012**, *52*, 3-4.
5. Matsui, K.; Boniface, J. J.; Steffner, P.; Reay, P. A.; Davis, M. M., Kinetics of T-cell receptor binding to peptide/I-Ek complexes: Correlation of the dissociation rate with T-cell responsiveness. *Proceedings of the National Academy of Science* **1994**, *91*, 12862-12866.

6. Tian, S.; Maile, R.; Collins, E., J; Frelinger, J. A., CD8+ T cell activation is governed by TCR-Peptide/MHC affinity, not dissociation rate. *Journal of Immunology* **2007**, *179*, 2952-2960.
7. McKeithan, T. W., Kinetic proofreading in T-cell receptor signal transduction. *Proceedings of the National Academy of Science* **1995**, *92* (11), 5042-6.
8. Rabinowitz, J. D.; Beeson, C.; Lyons, D. S.; Davis, M. M.; McConnell, H. M., Kinetic discrimination in T-cell activation. *Proceedings of the National Academy of Science* **1996**, *93*, 1401-1405.
9. Hahn, M.; Nicholson, M. J.; Pyrdol, J.; Wucherpfennig, K. W., Unconventional topology of self peptide–major histocompatibility complex binding by a human autoimmune T cell receptor. *Nature Immunology* **2005**, *6*, 490-496.
10. Sethi, D. K.; Schubert, D. A.; Anders, A.; Heroux, A.; Bonsor, D. A.; Thomas, C. P.; Sundberg, E. J.; Pyrdol, J.; Wucherpfennig, K. W., A highly tilted binding mode by a self-reactive T cell receptor results in altered engagement of peptide and MHC. *The Journal of Experimental Medicine* **2011**, *208* (1), 91-102.
11. Yin, Y.; Li, Y.; Mariuzza, R. A., Structural basis for self-recognition by autoimmune T-cell receptors. *Immunological Reviews* **2012**, *250*, 32-48.
12. Williams, C. B.; Engle, D. L.; Kersh, G. J.; White, J. M.; Allen, P. M., A kinetic threshold between negative and positive selection based on the longevity of the T cell receptor–ligand complex. *The Journal of Experimental Medicine* **1999**, *189* (10), 1531-1544.
13. Palmer, E., Negative selection--clearing out the bad apples from the T-cell repertoire. *Nature Reviews Immunology* **2003**, *3*, 383-391.
14. van der Merwe, A. P.; Davis, S. J., Molecular interactions mediating T cell antigen recognition. *Annual Review of Immunology* **2003**, *21*, 659-684.
15. Michel, F.; Attal-Bonnefoy, G.; Mangino, G.; Mise-Omata, S.; Acuto, O., CD28 as a molecular amplifier extending TCR ligation and signaling capabilities. *Immunity* **2001**, *15*, 935-945.
16. Acuto, O.; Michel, F., CD28-mediated co-stimulation: a quantitative support for TCR signalling. *Nature Reviews Immunology* **2003**, *12*, 939-951.
17. Sharpe, A. H., Mechanisms of costimulation. *Immunological Reviews* **2009**, *229* (1), 5-11.

18. Yokosuka, T.; Kobayashi, W.; Takamatsu, M.; Zeng, H.; Hashimoto-Tane, A.; Yagita, H.; Tokunaga, M.; Saito, T., Spatiotemporal basis of CTLA-4 costimulatory molecule-mediated negative regulation of T cell activation. *Immunity* **2010**, *33* (3), 326-339.
19. Yokosuka, T.; Kobayashi, W.; Sakata-Sogawa, K.; Takamatsu, M.; Hashimoto-Tane, A.; Dustin, M. L.; Tokunaga, M.; Saito, T., Spatiotemporal regulation of T cell costimulation by TCR-CD28 microclusters and protein kinase C theta translocation. *Immunity* **2008**, *29* (4), 589-601.
20. Singer, S. J., Intercellular communication and cell-cell adhesion. *Science* **1992**, *255* (5052), 1671-1677.
21. Bunnell, S. C.; Kapoor, V.; Tribble, R. P.; Zhang, W.; Samelson, L. E., Dynamic actin polymerization drives T cell receptor-induced spreading: a role for the signal transduction adaptor LAT. *Immunity* **2001**, *14* (3), 315-29.
22. Dustin, M. L., Cell adhesion molecules and actin cytoskeleton at immune synapses and kinapses. *Current Opinions in Cell Biology* **2007**, *19* (5), 529-33.
23. Springer, T. A.; Dustin, M. L., Integrin inside-out signaling and the immunological synapse. *Current Opinions in Cell Biology* **2012**, *24* (1), 107-15.
24. Huppa, J. B.; Axmann, M.; Mörtelmaier, M. A.; Lillemeier, B. F.; Newell, E. W.; Brameshuber, M.; Klein, L. O.; Schütz, G. J.; Davis, M. M., TCR-peptide-MHC interactions in situ show accelerated kinetics and increased affinity. *Nature* **2010**, *463* (7283), 963-7.
25. Huang, J.; Zarnitsyna, V. I.; Liu, B.; Edwards, L. J.; Jiang, N.; Evavold, B. D.; Zhu, C., The kinetics of two-dimensional TCR and pMHC interactions determine T-cell responsiveness. *Nature* **2010**, *464* (7290), 932-6.
26. Brian, A. A.; McConnell, H. M., Allogeneic stimulation of cytotoxic T cells by supported planar membranes. *Proceedings of the National Academy of Science* **1984**, *81*, 6159-6163.
27. Lin, W.-C.; Yu, C.-H.; Triffo, S.; Groves, J. T., Supported membrane formation, characterization, functionalization, and patterning for application in biological science and technology. **2010**, *2*, 235-269.
28. Yu, C.; Groves, J. T., Engineering supported membranes for cell biology. *Medical & Biological Engineering & Computing* **2010**, *48* (955-963).
29. Singer, S. J.; Nicolson, G. L., The fluid mosaic model of the structure of cell membranes. *Science* **1972**, *175* (4023), 720-731.

30. Grakoui, A.; Bromley, S. K.; Sumen, C.; Davis, M. M.; Shaw, A. S.; Allen, P. M.; Dustin, M. L., The immunological synapse: a molecular machine controlling T cell activation. *Science* **1999**, *285* (5425), 221-7.
31. Corr, M.; Slanetz, A. E.; Boyd, L. F.; Jelonek, M. T.; Khilko, S.; al-Ramadi, B. K.; Kim, Y. S.; Maher, S. E.; Bothwell, A. L.; Margulies, D. H., T cell receptor-MHC class I peptide interactions: affinity, kinetics, and specificity. *Science* **1994**, *265* (5174), 946-949.
32. Monks, C. R. F.; Freiberg, B. A.; Kupfer, H.; Sciaky, N.; Kupfer, A., Three-dimensional segregation of supramolecular activation clusters in T cells. *Nature* **1998**, *395* (6697), 82-86.
33. Nye, J. A.; Groves, J. T., Kinetic control of histidine-tagged protein surface density on supported lipid bilayers. *Langmuir* **2008**, *24* (8), 4145-4149.
34. Hartman, N. C.; Nye, J. A.; Groves, J. T., Cluster size regulates protein sorting in the immunological synapse. *Proceedings of the National Academy of Science* **2009**, *106*, 12729-12734.
35. Mossman, K. D.; Campi, G.; Groves, J. T.; Dustin, M. L., Altered TCR signaling from geometrically repatterned immunological synapses. *Science* **2005**, *310* (5751), 1191-1193.
36. Parthasarathy, R.; Yu, C.; Groves, J. T., Curvature-modulated phase separation in lipid bilayer membranes. *Langmuir* **2006**, *22* (5095-5099).
37. Groves, J. T.; Parthasarathy, R.; Forstner, M. B., Fluorescence imaging of membrane dynamics. *Annual Review of Biomedical Engineering* **2008**, *10*, 311-338.
38. Manz, B. N.; Jackson, B. L.; Petit, R. S.; Dustin, M. L.; Groves, J. T., T-cell triggering thresholds are modulated by the number of antigen within individual T-cell receptor clusters. *Proceedings of the National Academy of Science* **2011**, *108* (22), 9089-9094.
39. Smoligovets, A. A.; Smith, A. A.; Wu, H.-J.; Petit, R. S.; Groves, J. T., Characterization of dynamic actin associations with T-cell receptor microclusters in primary T cells. *Journal of Cell Science* **2012**, *125*, 735-742.
40. Yu, Y.; Fay, N. C.; Smoligovets, A. A.; Wu, H. J.; Groves, J. T., Myosin IIA modulates T cell receptor transport and CasL phosphorylation during early immunological synapse formation. *PLoS One* **2012**, *7* (2), e30704.

41. O'Donoghue, G. P.; Pielak, R. M.; Smoligovets, A. A.; Lin, J. J.; Groves, J. T., Direct single molecule measurement of TCR triggering by agonist pMHC in living primary T cells. *Elife* **2013**, *2*, e00778.
42. van der Merwe, P. A.; Dushek, O., Mechanisms for T cell receptor triggering. *Nature Reviews Immunology* **2011**, *11*, 47-55.
43. Deniz, A. A.; Mukhopadhyay, S.; Lemke, E. A., Single-molecule biophysics: at the interface of biology, physics and chemistry. *Journal of the Royal Society Interface* **2008**, *5* (15-45).

## Chapter 2

# Single Molecule Measurements of pMHC:TCR Binding in Self-Reactive Human T Cells

### Section 2.1: Introduction

Antigen discrimination by T cells occurs at the membrane-membrane interface between a T cell and an antigen-presenting cell. The presence of adhesion molecules at this junction influences its overall topography, which can significantly impact pMHC:TCR molecular interactions.<sup>1, 2, 3</sup> Existing measurements of ligand binding, such as surface plasmon resonance<sup>4, 5</sup> and mechanical assays,<sup>6</sup> do not account for the constraints and unique features of the intercellular junction and might not reflect the physiological T cell triggering environment. Due to the proposed role of the kinetics and affinity of self-pMHC binding to TCR in the pathogenesis of autoimmune disease,<sup>7, 8</sup> we are investigating two-dimensional pMHC:TCR interactions in live self-reactive human T cell clones in the context of a planar membrane-membrane interface.

Phenotype	TCR	MHC	Peptide
Normal	HA:D7	HLA-DR4	HA <sub>306-318</sub>
Self-Reactive	Ob.1A12	HLA-DR15	MBP <sub>85-99</sub>
Self-Reactive	Ob.2F3	HLA-DR15	MBP <sub>85-99</sub>
Self-Reactive	Hy.2E11	HLA-DR15	MBP <sub>85-99</sub>

**Table 2.1: Human T cell clones and their antigens.** The table describes the human T cell clones used in this study, highlighting their TCRs and corresponding peptide-MHC.

Here, we characterize the molecular interactions between pMHC and TCR in human T cell clones isolated from patients with multiple sclerosis (MS). Multiple sclerosis is an autoimmune disease that affects the central nervous system and specifically attacks the myelin sheath, an insulating layer surrounding neuronal axons.<sup>9</sup> One of the components of the myelin sheath, myelin basic protein (MBP), is a well-studied self-antigen that has been implicated in the autoimmune response in MS. The three self-reactive T cell clones used in this study, Ob.1A12,<sup>10</sup> Ob.2F3, and Hy.2E11, all recognize the MBP<sub>85-99</sub> peptide presented by the MS-associated HLA-DR15 MHC molecule (Table 2.1). The self-

antigen-MHC can trigger these clones with sufficient strength required to initiate and sustain an immune response. As a comparison, we are also examining pMHC:TCR binding in the influenza hemagglutinin (HA)-specific normal human T cell clone HA:D7, which recognizes the HA<sub>306-318</sub> peptide presented by HLA-DR4.<sup>11</sup>

## Section 2.2: Experimental setup

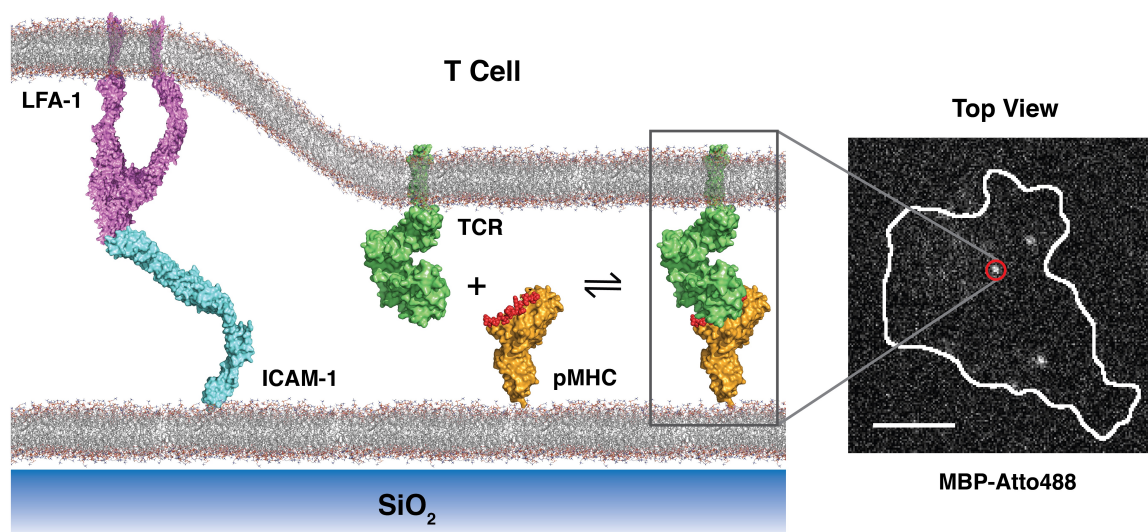


**Figure 2.1: Schematic of the hybrid live cell-supported membrane system.** The schematic shows the binding of the self-reactive TCR Ob.1A12 to its cognate pMHC, DR15-MBP (PDB, 1YMM). pMHC:TCR binding is observed via single molecule fluorescence microscopy at long exposure times (right) and aided by integrin adhesion between LFA-1 (PDB, 2K9J) and ICAM-1 (PDB, 1IAM, 1P53). pMHC molecules are labeled with Atto488 on the MBP peptide and detected using a 250 ms exposure time. Scale bar is 5  $\mu\text{m}$ .

We use hybrid live cell-supported membrane junctions to probe pMHC:TCR complex dynamics in human T cell clones (Figure 2.1).<sup>12</sup> Supported lipid bilayers are formed on glass coverslips<sup>13</sup> and functionalized with pMHC and the adhesion protein ICAM-1. The extracellular domain of human MHC (HLA-DR4 or HLA-DR15) is expressed with a BirA tag, allowing for site-specific enzymatic biotinylation at the C-terminus.<sup>14</sup> Monobiotinylated MHC is loaded with peptide (HA or MBP) and attached to lipids containing biotin head groups via biotin-streptavidin linkages. The extracellular domain of human ICAM-1 is expressed with a C-terminal decahistidine tag (His10) and attached to Ni-chelating lipids in the artificial membrane. T cells are added directly to this surrogate APC. Upon cell landing, the binding of ICAM-1 to LFA-1 on the cell surface leads to cell spreading and the formation of a planar interface between the T cell and artificial membrane, within which pMHC:TCR interactions occur.

In order to visualize pMHC molecules, the MHC is loaded with peptide covalently coupled in a 1:1 stoichiometry to the photostable fluorophore Atto488 using maleimide-thiol chemistry. The pMHC:TCR complexes are detected by imaging at long exposure times (250 ms), at which only the slow moving, bound pMHC molecules can be resolved.<sup>15</sup>

## Section 2.3: Peptide and protein preparation and characterization

### Section 2.3.1: Human antigen peptides

Peptide	Single Cysteine Variant Sequence
HA	PKYVKQNTLKAT <u>GGGC</u>
MBP	ENPVVHFFKNIVTPR <u>GGGC</u>

**Table 2.2: Peptide antigens and their sequences.** The table shows the two peptides used in this study, HA (nonself antigen for a healthy human T cell clone) and MBP (self antigen for three self-reactive human T cell clones). The peptide sequences are shown, with the nonnative addition of a single cysteine residue and flexible glycine linker underlined.

In this study, we use single cysteine variants of HA<sub>306-318</sub> and MBP<sub>85-99</sub> synthesized and purified by Elim Biopharmaceuticals. Each peptide variant includes a single cysteine residue at the C-terminus for the site-specific attachment of a fluorophore via maleimide-thiol chemistry. The cysteine is separated from the wild type peptide sequence via a flexible glycine trimer to prevent the fluorescent dye from perturbing the binding of the peptide to MHC or the binding of pMHC to TCR (Table 2.2). The peptide design is based on previous work showing that the addition of a C-terminal GGGC sequence in peptide antigens does not perturb function.<sup>15</sup>

The HA and MBP single cysteine peptides are fluorescently labeled by incubating them in a 1:2 molar ratio with Atto488 maleimide in phosphate buffer for 2 hours at room temperature. Figure 2.2A illustrates the maleimide-thiol peptide labeling reaction. The labeled peptides are purified on a C18 reverse phase column to remove unreacted dye and peptide (Figure 2.2B). MALDI-TOF mass spectrometry is then performed on fractions with absorbance at 280 nm and 488 nm to identify singly-labeled peptide. The peaks highlighted in gray correspond to the fractions containing labeled peptide as their major component and their mass spectra are shown (Figure 2.2C).

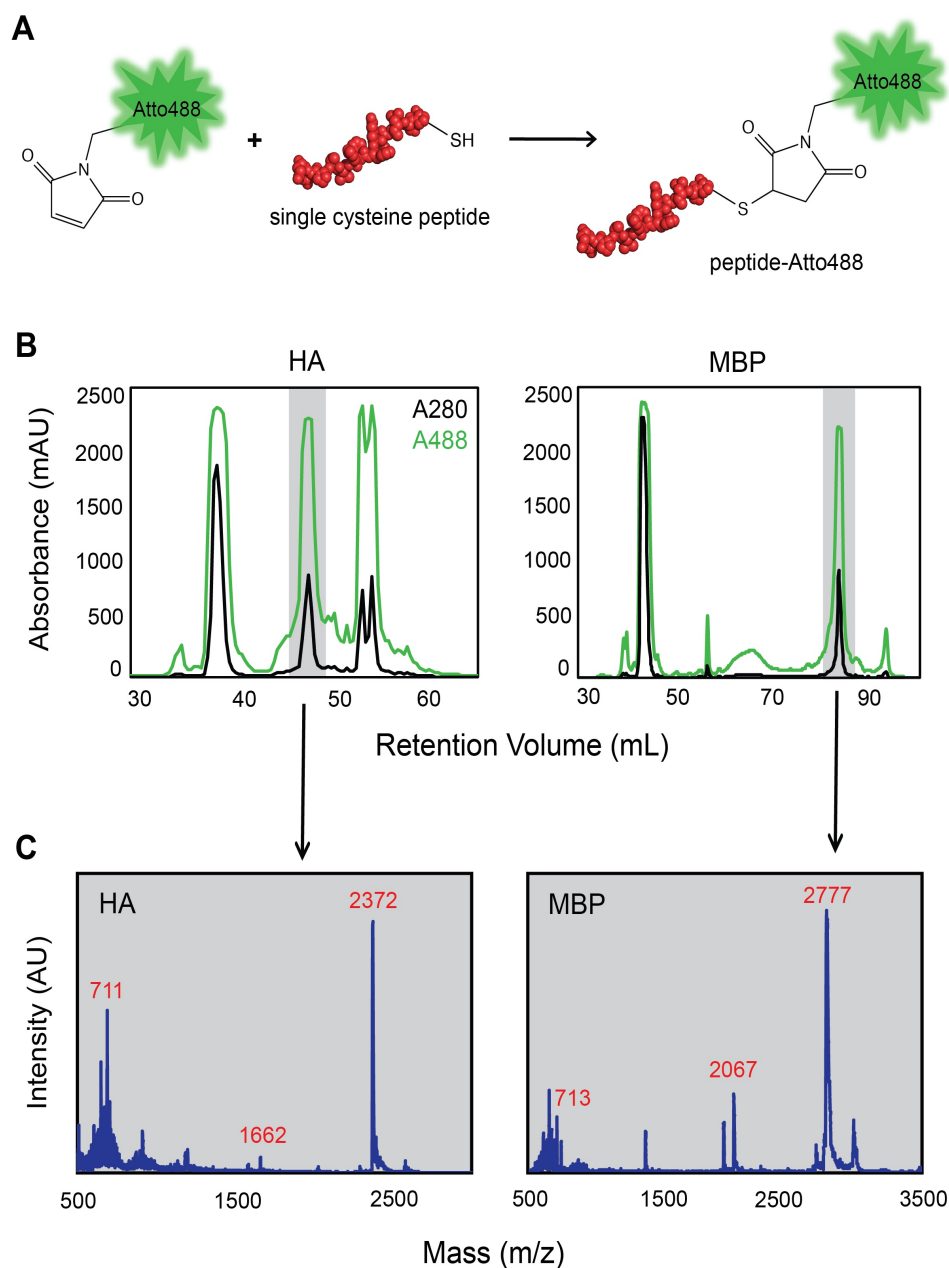


**Figure 2.2: Peptide labeling and purification.** (A) Schematic showing the maleimide-thiol reaction for labeling single cysteine variants of HA<sub>306-318</sub> and MBP<sub>85-99</sub> with Atto488 dye. (B) Reverse phase HPLC is used to separate labeled peptide from unreacted peptide and dye. The chromatograms show absorbances from the peptide (280 nm) and dye (488 nm). The gray areas highlight the fractions containing labeled peptide. (C) MALDI-TOF analysis of the gray peaks highlighted in (B). In each spectrum, the major peak corresponds to labeled peptide, confirming successful labeling and purification.

The major peak in the spectrum on the left (2372 m/z) is HA-Atto488, which has a molecular weight of 2377 g/mol. A small amount of free dye (712 g/mol) and unlabeled peptide (1665 g/mol) are observed, with peaks at 711 m/z and 1662 m/z. On the right, the major peak (2777 m/z) is MBP-Atto488, which has a molecular weight of 2783 g/mol. Minimal free dye and unlabeled peptide (2071 g/mol) remained in the fraction, with peaks at 713 m/z and 2067 m/z. We use the purified HA-Atto488 and MBP-Atto488 to load HLA-DR4 and HLA-DR15, respectively.

### **Section 2.3.2: Human pMHC characterization on a supported membrane**

The soluble human MHC proteins HLA-DR4 and HLA-DR15 were expressed with a C-terminal BirA tag in stably transfected Chinese hamster ovary cell lines. The molecules were purified using an anti-DR (L243) affinity matrix. Site-specific biotinylation of the BirA tag was performed overnight, excess biotin was removed by dialysis, and biotinylation was confirmed by gel shift with streptavidin on native polyacrylamide gels.<sup>16</sup> Purified HA-Atto488 and MBP-Atto488 discussed in the previous section were loaded onto HLA-DR4 and HLA-DR15, respectively, and unloaded peptide was separated by gel filtration. The soluble MHC II proteins were expressed, purified, biotinylated, and loaded by the Wucherpfennig group at Harvard University, as described previously.<sup>11</sup>

The monobiotinylated pMHC molecules used in this study had not previously been conjugated to a supported lipid bilayer for single molecule experiments. The streptavidin protein that links the biotin group on MHC to biotin on phospholipids in the membrane has four binding sites and thus has the potential to introduce artificial cross-linking.<sup>13</sup> While the pMHC densities required for single molecule experiments are very low (0.1-1 molecules/ $\mu\text{m}^2$ ) and may minimize the potential for cross-linking, it is important to characterize the oligomeric state of the protein before making quantitative measurements with T cells, as oligomerization could affect pMHC:TCR binding parameters. We use stepwise photobleaching to confirm that pMHC (DR4-HA-Atto488 and DR15-MBP-Atto488) is in its native monomeric state when linked to a supported membrane via biotin-streptavidin (Figure 2.3). This method relies on the irreversible and stochastic loss of fluorescence from repeated exposure of a fluorophore to a light source. The sample is continuously exposed to the excitation light at a low enough intensity that it is slowly bleached until its emission intensity is equivalent to the background fluorescence. Slow bleaching allows the temporal separation of multiple bleaching events, if present. Each bleaching event is represented as a step down in the intensity trace over time and the total number of steps is equivalent to the number of protein monomers in the molecule of interest. A monomeric protein coupled to a fluorophore in a 1:1 stoichiometry is represented as a single step down in fluorescence intensity, corresponding to the photobleaching of the single fluorophore attached to the molecule.<sup>17</sup>

Supported membranes used in this study are composed of 98% DOPC:2% Ni-NTA-DOGS:0.02% biotin-CAP-PE. The bilayers are incubated with 0.5  $\mu\text{g}/\text{mL}$  streptavidin for 45 minutes, rinsed, and then incubated with Atto488-pMHC for 35 minutes before a final rinse step. The protein-decorated bilayer is imaged using total internal reflection fluorescence (TIRF) microscopy at short exposure times (30 ms); a time lapse of images is recorded using a streaming acquisition rate. For each frame in a tracking sequence, single molecule diffraction-limited spots are detected by filtering for both size and intensity (Figure 2.3A) and linked into tracks using published particle detection and tracking algorithms adapted for MATLAB (Figure 2.3B, blue line).<sup>18</sup> Step photobleaching events are detected in an automated way using a Bayesian change point detection algorithm (Figure 2.3B, gray line).<sup>15, 19</sup>

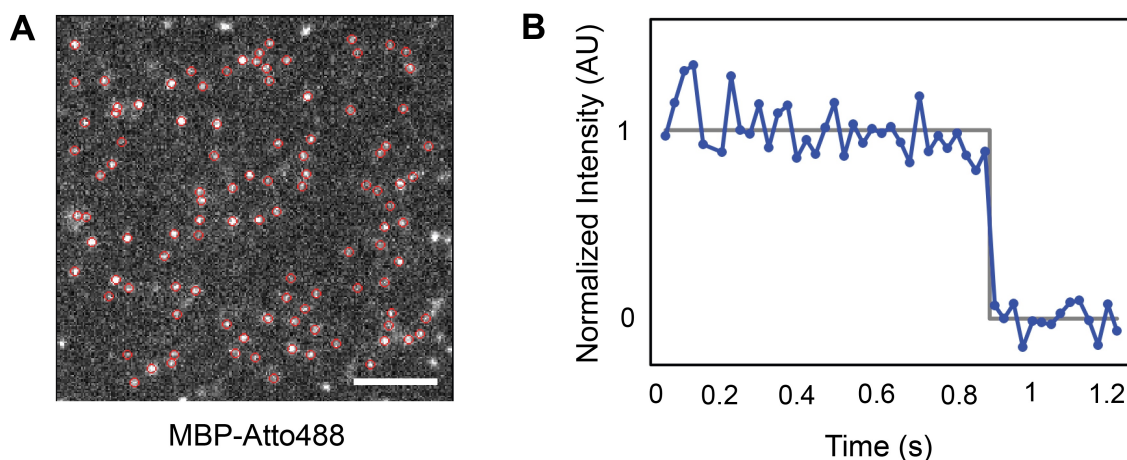


**Figure 2.3: pMHC is monomeric on the supported membrane.** Monobiotinylated pMHC does not form clusters when linked to a supported lipid bilayer via streptavidin. **(A)** Image shows one frame of a timelapse of DR15-MBP-Atto488 diffusing on a supported lipid bilayer. Single molecule diffraction-limited spots (in red) were detected in the image by filtering for both size and intensity and linked into tracks using published particle detection and tracking algorithms adapted for MATLAB. The scale bar is 5  $\mu\text{m}$  and the image was acquired using fast exposure times (30 ms). **(B)** Representative intensity trace (blue) showing a single pMHC molecule identified by step photobleaching. The trace represents a single puncta tracked in the timelapse corresponding to (A). The single step photobleaching event was detected in an automated way using a Bayesian change point detection algorithm (gray).

The timelapse data acquired for both DR4-HA-Atto488 and DR15-MBP-Atto488 show bright, mobile puncta diffusing on a supported membrane until they go dark from photobleaching. Figure 2.3A is one frame of a timelapse of DR15-MBP-Atto488 on a bilayer. The red circles represent the detected single molecule diffraction-limited spots, which were tracked over time to generate intensity traces. Figure 2.3B shows a representative single step photobleaching intensity trace for DR15-MBP-Atto488. The single step is indicative of a monomeric protein, confirming that streptavidin does not induce artificial cross-linking at low pMHC densities. Similar experiments were

performed with DR4-HA-Atto488, which also photobleaches in a single step. These results suggest that the biotinylated pMHC molecules DR15-MBP-Atto488 and DR4-HA-Atto488 are both mobile and monomeric when conjugated to an artificial membrane via biotin-streptavidin chemistry under the conditions used in this study.

### Section 2.3.3: ICAM-1 Purification and characterization on a supported membrane

A protein construct containing the extracellular domain of human ICAM-1 (residues 28-453) fused to a C-terminal decahistidine tag (ICAM-1-His10) was cloned into a pFastbac1 vector and introduced into the bac-to-bac insect cell/baculovirus based expression system according to manufacturer's directions and standard cloning procedures.<sup>20</sup> The protein was secreted from infected High5 cells and captured on Ni<sup>2+</sup>-nitrilotriacetic acid (NTA) agarose resin. The resin was washed and the protein was eluted using an imidazole gradient. The eluted fractions were analyzed via gel electrophoresis (SDS-PAGE, Figure 2.4), to determine which fractions predominantly contain ICAM-1-His10 and to evaluate the purity of the protein. The gel shows the fractions of interest, which each have a single major band of protein at ~ 50 kDa, as expected; the molecular weight of ICAM-1-His10 is 53 kDa. These protein fractions were combined and dialyzed to remove imidazole and stored in Tris buffer containing 10% glycerol.

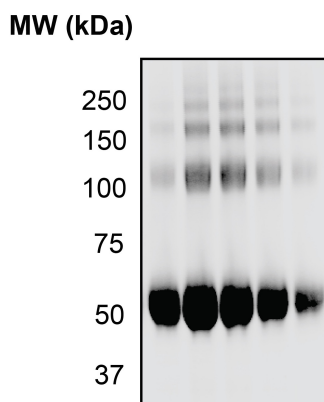


**Figure 2.4: Gel analysis of purified ICAM-1-His10.** Ruby-stained SDS-PAGE shows a single major band of protein at ~ 50 kDa for each eluted fraction, as expected.

Following purification, ICAM-1-His10 is characterized on a supported membrane to verify its mobility and function. The protein is fluorescently labeled at its lysine residues with Alexa Fluor 568 NHS ester and conjugated to a 98% DOPC:2% Ni-NTA-DOGS lipid bilayer via nickel chelation. Coupling of the protein to the bilayer is confirmed via fluorescence microscopy (epifluorescence).

Fluorescence recovery after photobleaching (FRAP) is used to verify the lateral mobility of the purified ICAM-1-His10 protein construct on a supported membrane (Figure 2.5A). Protein mobility is one of the physical parameters a cell experiences when interacting with a protein-decorated bilayer and it is important that the attached protein is homogeneously distributed and fluid to prevent effects from artificial clustering and membrane defects. FRAP is the most common method for characterizing two-dimensional lateral diffusion in thin films containing fluorescent probes. In this method, a small spot of the fluorescent sample is quickly photobleached by a short exposure to intense light. The fluorescence recovery, due to the replenishment of bleached probes by the surrounding fluorophores, is monitored over time.<sup>21</sup>

Figure 2.5A illustrates a successful ICAM-1-His10 FRAP experiment. A region of the ICAM-1-His10 bilayer was photobleached and the image on the left of Figure 2.5A was taken immediately following, showing a dark spot corresponding to photobleached ICAM-1. After three minutes, a second image was taken of the same bilayer region (Figure 2.5A, right). The image shows a homogeneous distribution of fluorescent protein due to the high lateral mobility of ICAM-1, which allowed the photobleached proteins to diffuse away and mix with bright proteins. Intensity traces of the two images were analyzed for the regions represented by the diagonal lines, showing ~100% fluorescence recovery and further demonstrating the high lateral mobility of ICAM-1-His10.

Previous studies have shown that Jurkat cells form the canonical immunological synapse<sup>22</sup> when interacting with a supported lipid bilayer containing TCR stimulatory molecules (anti-CD3) and ICAM-1.<sup>23</sup> Here, we utilize Jurkat cells to investigate the function of the human ICAM-1-His10 construct and verify its ability to bind LFA-1 on human T cells and form a pSMAC. Supported membranes are prepared from SUVs consisting of 98% DOPC:2% Ni-NTA-DOGS:0.02% biotin-CAP-PE. To stimulate the Jurkat cells, monoclonal antibodies to the CD3 $\epsilon$  subunit of TCR (anti-CD3) are biotinylated and linked to the bilayer via biotin-streptavidin. ICAM-1 is coupled to the bilayer via nickel chelation and the membrane is incubated with Jurkat cells for 30 minutes before epifluorescence imaging. Both anti-CD3 and ICAM-1 are fluorescently labeled at their lysine residues with Alexa Fluor 647 NHS ester (anti-CD3) or Alexa Fluor 568 NHS ester (ICAM-1) to allow visualization. After 30 minutes, the majority of cells (~75%) form a bulls eye pattern consisting of a large, central cluster of stimulatory antibodies surrounded by a zone of ICAM-1 enrichment (Figure 2.5B). These results indicate that the human ICAM-1-His10 construct is functional when attached to a supported lipid bilayer due to its ability to bind LFA-1 on a stimulated T cell and form the canonical pSMAC.

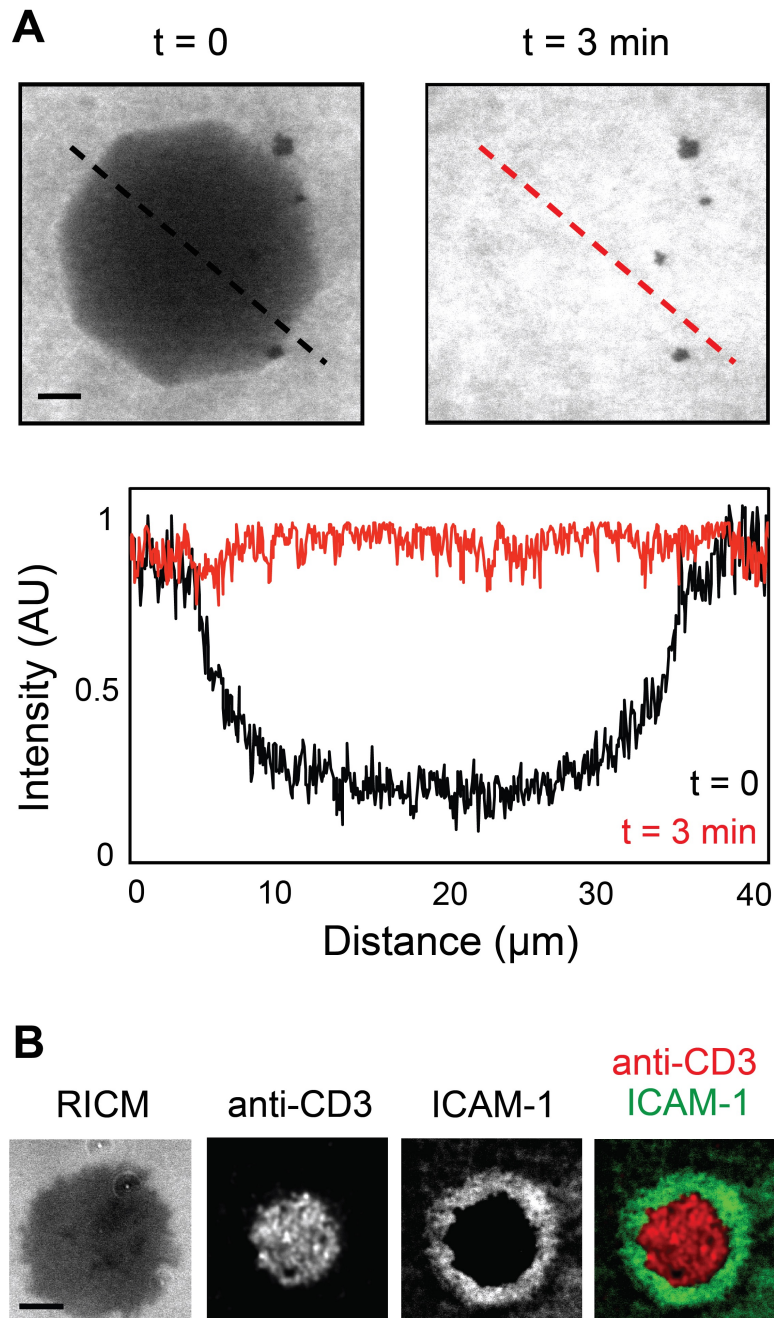


**Figure 2.5: Characterization of ICAM-1-His10 on a supported membrane.** (A) Representative FRAP characterization of a supported membrane conjugated with ICAM-1-His10 demonstrates the lateral mobility of the protein. The diagonal lines represent the region shown in the intensity trace. (B) A representative Jurkat cell bound to the lipid bilayer showing an immunological synapse 30 minutes after stimulation was initiated. RICM shows the cellular footprint and epifluorescence was used to image anti-CD3 and ICAM-1. Scale bars are 5  $\mu\text{m}$ .

## Section 2.4: Single molecule measurements of pMHC:TCR kinetics and affinity in self-reactive human T cell clones

### Section 2.4.1: Direct observations of pMHC:TCR binding

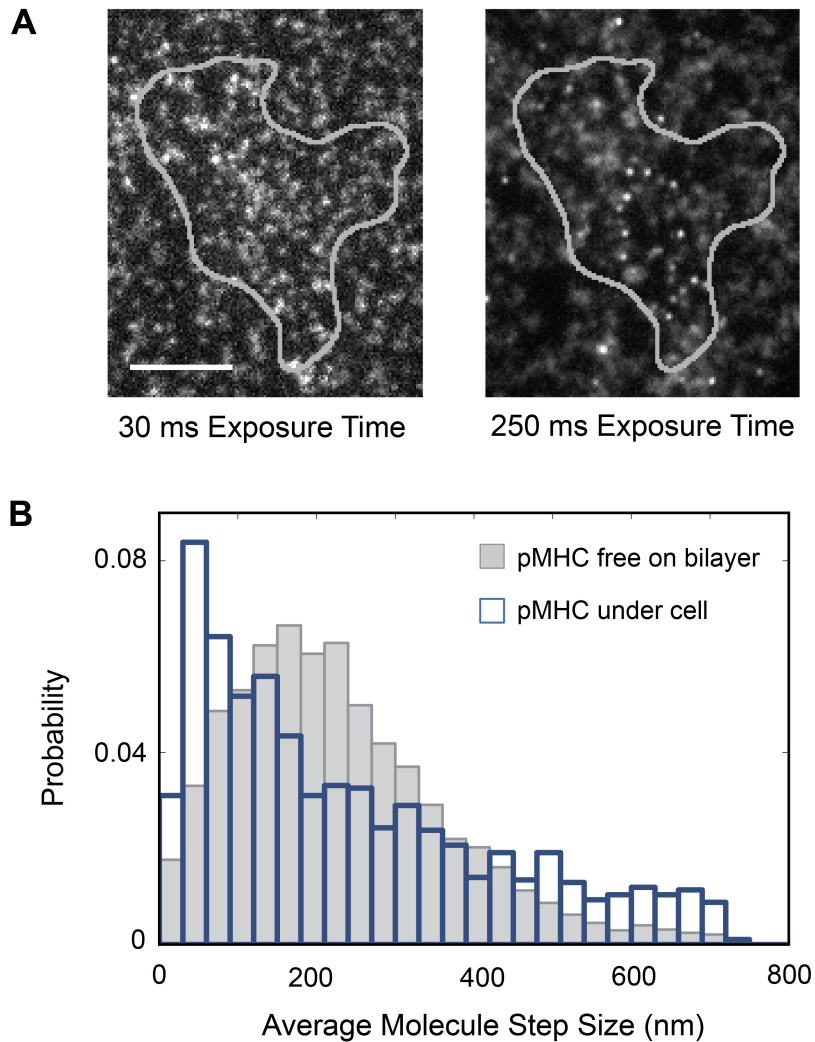


**Figure 2.6: pMHC binding to TCR in live T cells is revealed by changes in mobility. (A)** Imaging at long exposure times (250 ms, right) allows for discrimination between the slow, TCR bound fraction of pMHC and the fast diffusing fraction. HA:D7 with DR4-HA-Atto488 binding is shown, with the cell boundary depicted as a gray line. Scale bar is 5 $\mu$ m. **(B)** The change in the step size of single pMHC molecules due to binding events is further illustrated by the histogram, which shows a decrease in average molecular step size for molecules under the cell compared to molecules in the absence of T cells.

Binding events between fluorescently-labeled pMHC on supported membranes and TCR on human T cell clones are revealed by changes in molecular mobility.<sup>15</sup> At short exposure times (30 ms), all molecules on the bilayer are readily resolved (Figure 2.6A, left). In regions without a cell, tracked pMHC molecules exhibit a unimodal step-size distribution, centering around 200 nm (Figure 2.6B, gray). Within the T cell junction, the step-size distribution becomes roughly bimodal, with a peak at  $\sim 200$  nm and a second peak at  $\sim 50$  nm. The peak at 50 nm corresponds to slow-moving, bound pMHC. The slow-moving, bound fraction of molecules is readily distinguished from freely diffusing pMHC by imaging at long exposure times (250 ms, Figure 2.6A, right). The T cell boundary is determined by reflection interference contrast microscopy (RICM) and is depicted as a gray line.

### Section 2.4.2: Single molecule pMHC:TCR binding kinetics

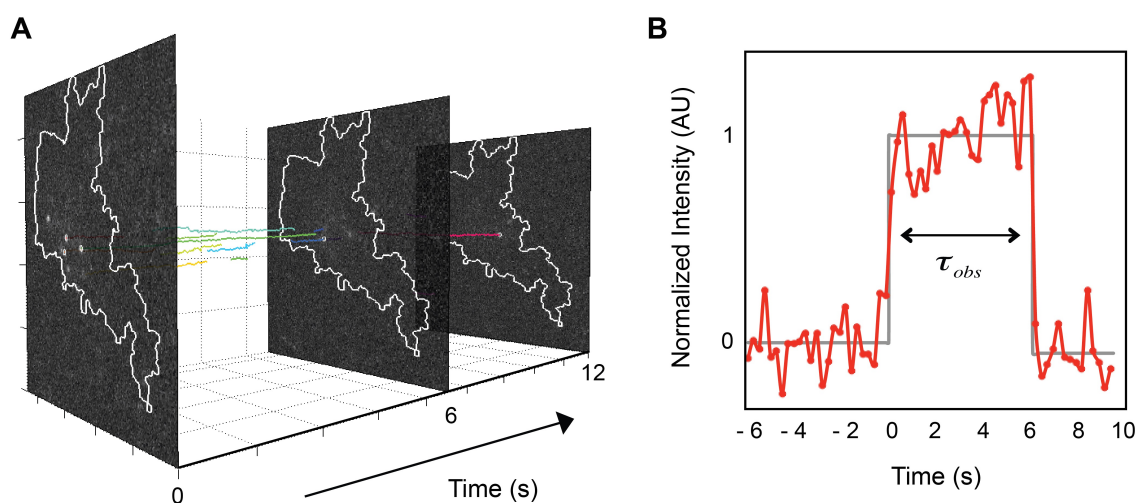


**Figure 2.7: Tracking single molecule pMHC:TCR binding events in a self-reactive human T cell clone.** (A) A 3D spatial map of the bound MBP-Atto488 single molecule puncta tracked from a single Ob.1A12 T cell clone over 12 s. Each color represents a different pMHC:TCR single molecule trajectory. Trajectories beginning at later time points represent *de novo* receptor:ligand binding events. (B) Representative intensity trace showing a single pMHC molecule from (A), identified by step photobleaching and bound continuously for  $\sim 6$  s, which we call  $\tau_{obs}$ .

Using the time-resolved single molecule fluorescence microscopy technique described previously, we can unambiguously track individual pMHC:TCR complexes as they move within the T cell junction over time. A sequence of images is recorded using streaming acquisition or 1-3 s time lapses, depending on the clone, and single molecule diffraction-limited spots are detected by filtering for both size and intensity and linked into tracks.<sup>15</sup>

Figure 2.7A is a 3D spatial map of the bound MBP-Atto488 single molecule puncta tracked from a single Ob.1A12 T cell clone over 12 s. The figure shows select frames in the imaging sequence, with trajectories of pMHC:TCR complexes depicted as colored lines moving along the time axis. Each color represents a different pMHC:TCR single molecule trajectory lasting fractions of a second up to  $\sim 6$  seconds. Trajectories beginning at later time points represent *de novo* receptor:ligand binding events. By tracking the fluorescence intensity of Atto488-pMHC over time, we can visualize individual binding and unbinding events as step changes in intensity compared to the background bilayer fluorescence (Figure 2.7B). The total time between the intensity step-up (binding) and step-down (unbinding) is the observed dwell time,  $\tau_{obs}$ , for the individual complex.

Unbinding and photobleaching are indistinguishable in fluorescence methods such as this, and both events appear as a single step down in intensity. Thus, the observed dwell time is the result of both unbinding and photobleaching events. We can write the observed unbinding rate ( $k_{obs}$ ), which is the inverse of  $\tau_{obs}$ , as the summation of the unbinding rate,  $k_{off}$ , and the photobleaching rate,  $k_{bl}$ ,

$$k_{obs} = k_{off} + k_{bl}. \quad (2.1)$$

It follows that the observed dwell time is represented by the equation,

$$\tau_{obs} = \left( (\tau_{off})^{-1} + (\tau_{bl})^{-1} \right)^{-1}. \quad (2.2)$$

By measuring both  $\tau_{obs}$  and  $\tau_{bl}$  it is possible to calculate the molecular binding dwell time,  $\tau_{off}$ , as long as  $\tau_{obs} < \tau_{bl}$ .

We tracked over 900 pMHC:TCR complexes for each human T cell clone and measured their single molecule pMHC:TCR dwell time distributions (Figure 2.8A). The observed dwell time distributions for all clones are exponential, in agreement with previously published results for pMHC:TCR dwell times in primary mouse T cells.<sup>15</sup> The distribution of observed dwell times is described by the two-component exponential equation,

$$f(\tau_{obs}) = \left( \langle \tau_{bl} \rangle^{-1} + \langle \tau_{off} \rangle^{-1} \right) e^{-\tau_{obs} (\langle \tau_{bl} \rangle^{-1} + \langle \tau_{off} \rangle^{-1})}, \quad (2.3)$$

where  $\langle \tau_{bl} \rangle$  and  $\langle \tau_{off} \rangle$  are the mean bleaching time and mean molecular binding dwell time, respectively.<sup>15</sup> Bleaching times are measured by immobilizing Atto488-pMHC on glass slides and imaging using identical conditions as for dwell time experiments. These times are significantly longer than observed dwell times for all TCRs. As an example, Figure 2.8B shows the observed dwell time distribution for Ob2.F3 binding Atto488-MBP-DR15, as well as the Atto-488-MBP-DR15 bleaching time distribution. The plot

illustrates that the bleaching times are significantly longer than the observed dwell times when measured using a 1 s time lapse. Thus, we are confident that we are measuring molecular unbinding events in our assay.

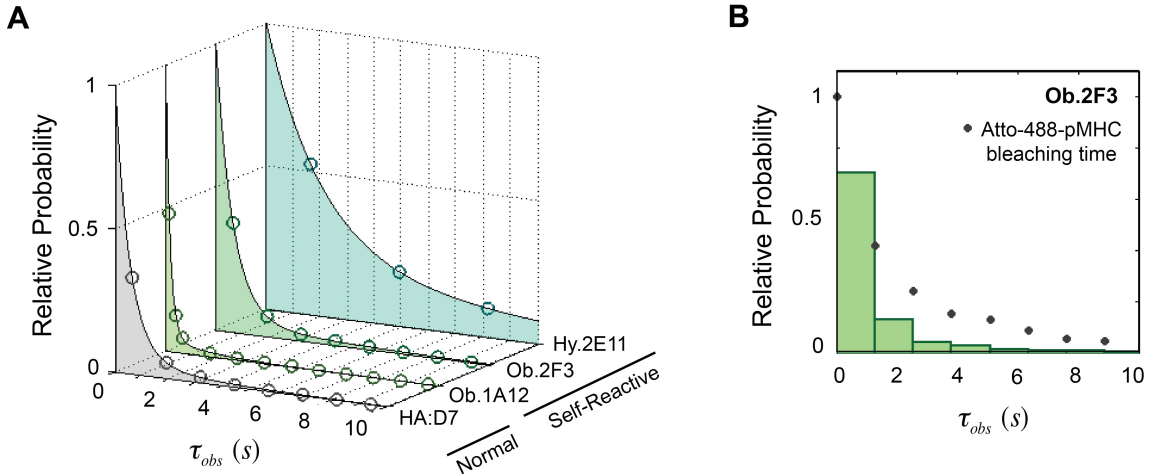


**Figure 2.8: The distribution of observed pMHC:TCR dwell times in human T cell clones.**

(A) Observed dwell time distributions ( $\tau_{obs}$ ) for the TCRs HA:D7, Ob.1A12, Ob.2F3, and Hy.2E11 binding to DR15-MBP-Atto488 or DR4-HA-Atto488. Distributions are exponential for all T cell clones. Data for dwell time distributions represent  $> 900$  pMHC molecules tracked for each clone from a population of 8-12 cells. (B) Photobleaching is slower than observed dwell times. The distribution of pMHC:TCR dwell times for Ob.2F3 is shown as an example, with bleaching times,  $\tau_{bl}$ , (gray circles) of Atto488-pMHC taken under the same imaging conditions plotted.

We measure the mean bleaching times and observed dwell times for each human T cell clone and use them to calculate the molecular binding dwell times for pMHC:TCR complexes using the equation

$$\langle \tau_{off} \rangle = \frac{\langle \tau_{bl} \rangle \langle \tau_{obs} \rangle}{\langle \tau_{bl} \rangle - \langle \tau_{obs} \rangle}. \quad (2.4)$$

This data is summarized in Table 2.3 and illustrates that there is no apparent relationship between self-reactivity and dwell time.

Phenotype	TCR	Antigen	Imaging Condition	$\langle\tau_{obs}\rangle$ (s)	$\langle\tau_{bl}\rangle$ (s)	$\langle\tau_{off}\rangle$ (s)
Normal	HA:D7	DR4-HA	Streaming	1.0	1.6	2.7
Self-Reactive	Ob.1A12	DR15-MBP	3s	5.2	17.7	7.3
Self-Reactive	Ob.2F3	DR15-MBP	1 s	2.3	7.4	3.4
Self-Reactive	Hy.2E11	DR15-MBP	3 s	9.7	17.7	21.5

**Table 2.3: Mean molecular binding dwell times for human T cell clones.** The table shows the mean molecular binding dwell times,  $\langle\tau_{off}\rangle$ , that were calculated from mean observed dwell times,  $\langle\tau_{obs}\rangle$ , and mean photobleaching times,  $\langle\tau_{bl}\rangle$ , for each T cell clone.

### Section 2.4.3: Single molecule pMHC:TCR binding affinity

The single molecule binding assay also allows us to examine the *in situ* binding affinities of the four TCRs to their respective pMHC ligand. The dissociation constant for pMHC:TCR binding is described by the equation,

$$K_D = \frac{\rho(pMHC_{total})\rho(TCR)}{\rho(pMHC:TCR)}, \quad (2.5)$$

where  $\rho(pMHC_{total})$  is the total density of pMHC in the T cell junction,  $\rho(TCR)$  is the total density of TCR in the junction, and  $\rho(pMHC:TCR)$  is the density of pMHC:TCR complexes in the junction.  $\rho(pMHC_{total})$  can be determined using short exposure times, while  $\rho(pMHC:TCR)$  can be determined using long exposure times. Because the TCR surface expression levels for all clones is comparable,  $\rho(TCR)$  can be omitted for the purpose of comparing the affinities of the different clones.<sup>11</sup> Finally, because the  $pMHC_{total}$  and pMHC:TCR surface densities pertain to the same area, the area of the T cell junction within the artificial membrane as determined by RICM, the area cancels and we can simply calculate the number of  $pMHC_{total}$  and the number of pMHC:TCR complexes in order to measure binding affinity for each clone. The parameter that we are interested in calculating is the binding efficiency, or fraction of pMHC that is bound to TCR, and can be represented by the equation:

$$Binding\ Efficiency = \frac{pMHC:TCR}{pMHC_{total}}. \quad (2.6)$$

The number of bound pMHC for a single cell is measured by counting the puncta that lie within the cell boundary when imaged using a 250 ms exposure time. The total number of

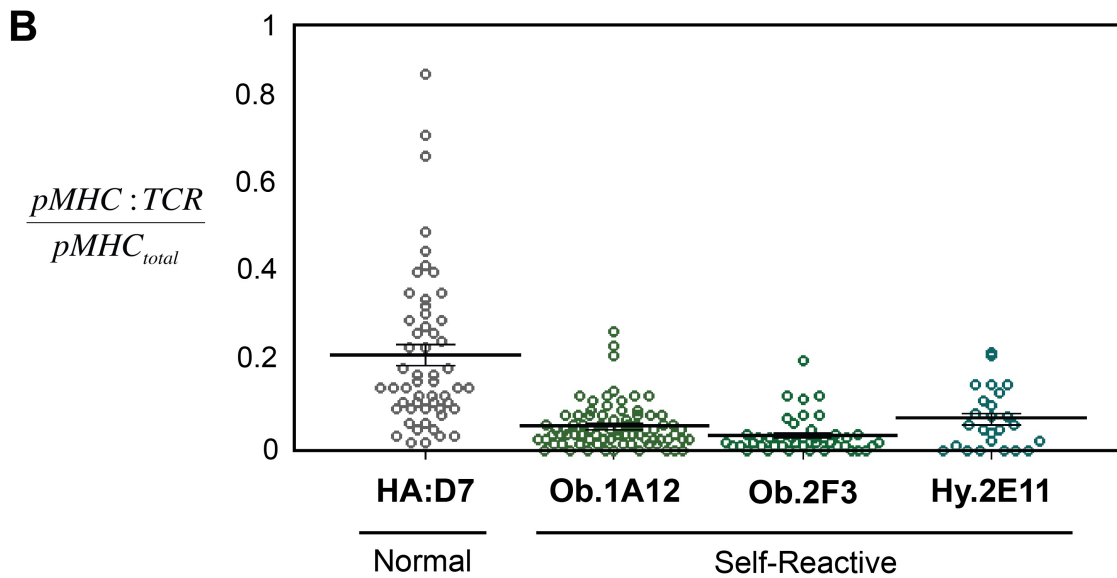
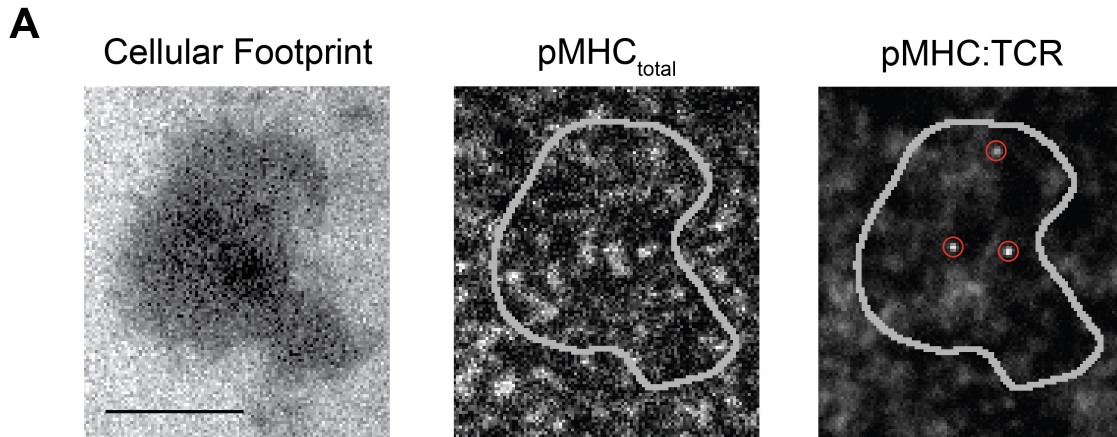


**Figure 2.9: Self-reactive T cell clones have a lower TCR affinity for pMHC.** (A) The number of bound pMHC for a single cell is measured by counting the puncta that lie within the cell boundary, as determined by RICM (cellular footprint). Bound pMHC are observed using a 250 ms exposure time. The total number of pMHC at the cell interface is calculated from the total fluorescence intensity within the cell boundary. Total pMHC are observed using a 30 ms exposure time. Representative images of Ob.1A12 with bound DR15-MBP-Atto488 are shown. Scale bar is 5  $\mu$ m. (B) Distributions of the fraction of bound pMHC for HA:D7, Ob.1A12, Ob.2F3, and Hy.2E11 show a higher pMHC:TCR affinity for HA:D7 compared to the self-reactive clones. Plots represent data from 26-81 cells for each clone.

pMHC at the cell interface is calculated from the total fluorescence intensity within the cell boundary, determined using a 30 ms exposure time. Figure 2.9A illustrates this calculation, showing an Ob.1A12 cell with DR15-MBP-Atto488 on the supported membrane. Binding efficiencies were examined for all T cell clones, imaging > 25 cells

per clone (Figure 2.9B). These results show the distribution of efficiencies for each clone. The normal T cell clone, HA:D7, displays a wide range of binding efficiencies, between 0.02 and 0.9. In contrast, all three self-reactive clones exhibit a much smaller range of efficiencies, between 0 and  $\sim 0.2$ - $0.3$ . In addition to having a wider spread, HA:D7 also has a higher mean binding efficiency compared to the self-reactive clones (Table 2.4). These results agree with previous affinity measurements for all four clones, which reported a 2D affinity for HA:D7 that was  $\sim 10$ -fold higher than that of the self-reactive human T cells.<sup>11</sup>

## Section 2.5: Discussion and conclusions

Phenotype	TCR	Antigen	$\langle \tau_{off} \rangle$ (s)	$\frac{pMHC:TCR}{pMHC_{total}}$
Normal	HA:D7	DR4-HA	2.7	0.2
Self-Reactive	Ob.1A12	DR15-MBP	7.3	0.05
Self-Reactive	Ob.2F3	DR15-MBP	3.4	0.03
Self-Reactive	Hy.2E11	DR15-MBP	21.5	0.07

**Table 2.4: Molecular binding dwell times and binding efficiencies for human T cell clones.** Molecular binding dwell times and mean binding efficiencies for the TCRs HA:D7, Ob.1A12, Ob.2F3, and Hy.2E11 binding to DR15-MBP-Atto488 or DR4-HA-Atto488.

In this study, we report the first single molecule kinetics measurements in self-reactive human T cells. Prior kinetics studies of the pMHC:TCR interactions for the HA:D7, Ob.1A12, Ob.2F3, and Hy.2E11 human T cell clones were limited to three-dimensional solution assays and two-dimensional mechanical assays. Of the four T cell clones used in this study, surface plasmon resonance kinetic data only exists for Ob.1A12 and Hy.2E11 TCRs binding their DR15-MBP ligands. DR15-MBP:Ob.1A12 binding was characterized by a  $K_D$  of  $81 \mu\text{M}$  and a  $k_{off}$  of  $0.17 \text{ s}^{-1}$  ( $\tau_{off} = 5.9 \text{ s}$ ), while DR15-MBP:Hy.2E11 binding was characterized by a  $K_D$  of  $123 \mu\text{M}$  and a  $k_{off}$  of  $0.73 \text{ s}^{-1}$  ( $\tau_{off} = 1.4 \text{ s}$ ).<sup>24</sup> While SPR data for the DR4-HA:HA:D7 interaction does not exist, the typical affinity range reported for TCRs binding to foreign agonist pMHCs is  $K_D \sim 1\text{--}50 \mu\text{M}$ .<sup>25</sup> The two-dimensional off-rates and relative affinities of the pMHC:TCR interactions for the HA:D7, Ob.1A12, Ob.2F3, and Hy.2E11 human T cell clones have been determined using the micropipette adhesion frequency assay.<sup>26, 27, 6</sup> This technique measured a ten-fold higher affinity for HA:D7 binding its antigen compared to all three self-reactive clones. In contrast, the measured 2D off-rates were the same or similar for all clones. HA:D7, Ob.1A12, and

Ob.2F3 binding their antigens had a  $k_{off}$  of  $1.2 \text{ s}^{-1}$  ( $\tau_{off} = 0.83 \text{ s}$ ) and the DR15-MBP:Hy.2E11 interaction had a  $k_{off}$  of  $1.1 \text{ s}^{-1}$  ( $\tau_{off} = 0.91 \text{ s}$ ).<sup>11</sup>

Table 2.4 summarizes the molecular binding dwell times and binding efficiencies determined via time-resolved single molecule methods using a hybrid live T cell-supported membrane system. In agreement with the micropipette adhesion frequency results, as well as trends from SPR studies, we showed that the self-reactive TCRs bind their cognate antigen-MHC with a lower affinity compared to the normal, influenza-specific TCR, HA:D7. In contrast, our dwell time results do not agree with prior 2D kinetics measurements. The discrepancies between the adhesion frequency assay and our technique can be explained by the escape directions in the different pMHC:TCR binding environments (Figure 2.10). In the micropipette adhesion frequency method, a T cell is held in one micropipette and a glass bead or red blood cell coated with pMHC is held in a second micropipette. T cells are micro-manipulated to touch the red blood cell or bead with a controlled contact area and time. The binding of TCR to pMHC results in elongation of the red blood cell or T cell upon withdrawal, and this process is repeated many times to obtain an adhesion frequency from which kinetic rates can be derived.<sup>11</sup> As shown in Figure 2.10, this technique allows for precise vertical control of the pMHC:TCR interaction, but no lateral freedom. Any measured unbinding may be due to the force of pulling on the micropipette, which could result in artificially shortened and similar dwell times for a panel of pMHC:TCR pairs. The use of supported membrane-T cell junctions is more similar to the physiological juxtacrine signaling environment, and thus the measured pMHC:TCR kinetics are more representative of the receptor:ligand interactions during T cell signaling. This system is characterized by both vertical and lateral escape directions, as the pMHC molecules can move freely on the supported lipid bilayer. Such lateral movements may contribute to differences in unbinding in the single molecule results reported here. In addition to the differences in escape directions between the two systems for measuring two-dimensional pMHC:TCR kinetics, the discrepancies in molecular binding dwell times may also arise from other environmental and biological effects, including the influence of integrins on pMHC:TCR interactions. ICAM-1:LFA-1 binding aids in T cell spreading and the creation of a planar, highly constrained interface at which pMHC:TCR binding occurs.<sup>28, 29</sup>

Likely, the differences in measured two-dimensional kinetic parameters result from a combination of effects originating from the techniques and their presentation of pMHC. The work presented here highlights the significance of investigating pMHC:TCR interactions in a system most similar to the native T cell-APC junction, as the nature of environmental influences on molecular binding cannot be readily predicted.<sup>30</sup>

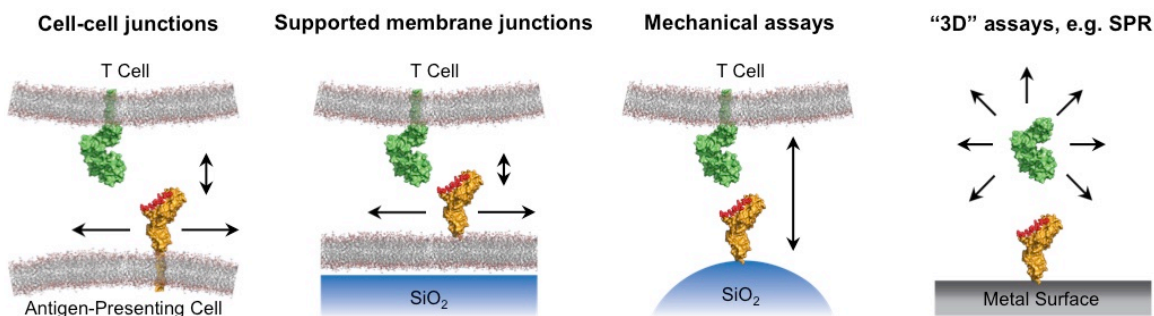


**Figure 2.10: Escape directions in different pMHC:TCR binding environments.** The schematics compare the physiological T cell signaling environment to three different experimental systems used to measure pMHC:TCR kinetics. The arrows indicate the escape directions of unbinding events. T cell signaling occurs at cell-cell junctions between T cells and antigen-presenting cells (far left). This signaling junction provides a juxtacrine geometry, physiological lateral fluidity, and physiological vertical freedom. Supported membrane junctions between a T cell and supported lipid bilayer functionalized with pMHC (middle left) and mechanical assays using a T cell interfaced with a pMHC-coated glass bead or red blood cell (middle right) both provide juxtacrine geometries. Supported membrane junctions also have high lateral fluidity and negligible vertical freedom, while mechanical assays allow for no lateral freedom and precise vertical control. 3D assays, such as SPR (far right), provide a paracrine geometry and isotropic fluidity.

## Section 2.6: Materials and methods

### Section 2.6.1: Cell culture

Jurkat clone E-61 was purchased from the American Type Culture Collection (Manassas, VA) and cultured in RPMI 1640 supplemented with 10% FBS, 2 mM L-glutamine, 10 mM HEPES, 1 mM sodium pyruvate, and Pennicillin-Streptomycin (all Life Technologies, South San Francisco, CA).

The human T cell clones HA:D7, Ob.1A12, Ob.2F3, and Hy.2E11 were a gift of Kai Wucherpfennig, Dana-Farber Cancer Institute and Harvard Medical School, Boston, MA. Self-reactive T cell clones Ob.1A12, Ob.2F3, and Hy.2E11 (recognizing MBP<sub>85-99</sub>-HLA-DR15 [DRB1\*15:01]) were previously isolated from patients with relapsing-remitting MS.<sup>10</sup> T cell clone HA:D7 was previously sorted from peripheral blood mononuclear cells from healthy donors using HLA-DR0401-HA<sub>306-318</sub> tetramers after in vitro expansion.<sup>11</sup> Human T cell clones were restimulated with PHA-L (Roche, Basel, Switzerland) in the presence of irradiated peripheral blood mononuclear cells (StemExpress LLC, Placerville, CA) and cultured in RPMI 1640 supplemented with 10% FBS, 2 mM GlutaMAX-I, 10 mM HEPES (all Life Technologies, South San Francisco, CA), 1% human serum (Valley Biomedical, Winchester, VA), and 5 U/ml rIL-2 (Roche), as previously described.<sup>11</sup> T cells were used between days 11 and 14 after restimulation.

### **Section 2.6.2: Protein expression and purification**

Soluble MHC class II proteins were a gift of Kai Wucherpfennig, Dana-Farber Cancer Institute and Harvard Medical School, Boston, MA. HLA-DR15 and HLA-DR4 were expressed, purified, loaded with fluorescently labeled peptide (MBP-Atto488 or HA-Atto488), and BirA biotinylated as previously described.<sup>11, 16</sup> MHC loaded with peptide (pMHC) was stored in Tris buffer containing 10% glycerol.

A plasmid containing human ICAM-1 was a gift from Timothy Springer (Addgene plasmid # 8632).<sup>20</sup> A decahistidine-tagged human ICAM-1 protein was generated by PCR amplifying the ICAM-1 extracellular domain sequence and subcloning it into a pFastBac1 vector (Life Technologies, Carlsbad, CA). The protein was expressed in High5 insect cells (UC Berkeley Tissue Culture Facility) and purified by Ni<sup>2+</sup>-nitrilotriacetic acid (NTA) agarose (Qiagen, Venlo, Netherlands) affinity column, eluted with an imidazole gradient, dialyzed, and stored in Tris buffer containing 10% glycerol.

### **Section 2.6.3: Peptide purification and labeling**

Using the sequences of myelin basic protein (MBP; amino acids 85-99)<sup>10</sup> and influenza hemagglutinin (HA; amino acids 306-318),<sup>31</sup> the following single cysteine peptide variants were synthesized commercially (Elim Biopharmaceuticals, Hayward, CA): MBP(C) (ENPVVHFFKNIVTPRGGGC) and HA(C) (PKYVKQNTLKATGGGC). For fluorophore labeling, peptides were dissolved in a small amount of phosphate buffer and mixed in a 1:2 molar ratio with lyophilized Atto488 maleimide (Atto-Tec GmbH, Siegen, Germany). The peptides were then incubated at room temperature for 2 hours and purified on a C18 reverse phase column (Grace-Vydac, Deerfield, IL) and H<sub>2</sub>O:acetonitrile gradient using an AKTA explorer 100 FPLC system (Amersham Pharmacia Biotech, Piscataway, NJ). Peptide identity and attachment of a single fluorophore were confirmed after purification using MALDI-TOF mass spectrometry (Voyager DE Pro; Applied Biosystems, Foster City, CA).

### **Section 2.6.4: Antibody preparation**

Purified mouse anti-human CD3 (clone HIT3a) was purchased from BD Biosciences (Franklin Lakes, NJ) and biotinylated using the EZ-Link-Sulfo-NHS-LC-Biotin Kit (Thermo Fisher Scientific, Waltham, MA) following the manufacturer's protocol for attachment of 1-3 biotin groups per antibody. Biotinylated antibody was washed with PBS using 10,000 MWCO spin concentrators (Vivaspin 500, GE Health Care, Pittsburgh, PA) to remove unreacted biotin and fluorescently labeled with Alexa Fluor 647 Monoclonal Antibody Labeling Kit (Life Technologies, South San Francisco, CA).

## Section 2.6.5: Imaging chamber and supported lipid bilayer preparation

Small unilamellar vesicles (SUVs) were formed by tip sonication of a solution composed of 98 mol % 1,2-dioleoyl-*sn*-glycero-3-phosphocholine (DOPC), 2 mol % 1,2 dioleoyl-*sn*-glycero-3-[(N-(5-amino-1-carboxypentyl) iminodiacetic acid) succinyl] (nickel salt) (Ni-NTA-DOGS), and 0.02 mol % 1,2-dioleoyl-*sn*-glycero-3-phosphoethanolamine-N-(cap biotinyl) (sodium salt) (18:1 Biotinyl Cap PE) (Avanti Polar Lipids, Alabaster, AL) in Milli-Q water (EMD Millipore, Billerica, MA). Tip sonication was preferred to vesicle extrusion due to the introduction of significant levels of fluorescent impurities into the SUVs during extrusion. Prior to experiments, #2 40 mm diameter round coverslips were ultrasonicated for 30 min in 50:50 isopropyl alcohol:water, rinsed thoroughly in Milli-Q water (EMD Millipore, Billerica, MA), etched for 5 min in piranha solution (3:1 sulfuric acid:hydrogen peroxide), and again rinsed thoroughly in Milli-Q water. The coverslips were used in the assembly of FCS2 Closed Chamber Systems (flow cells; Bioprotech, Butler, PA), which were pre-filled with Tris-buffered saline (TBS; 19.98 mM Tris, 136 mM NaCl, pH 7.4; Mediatech Inc., Herndon, VA). SUVs were then flowed into the chambers, and bilayers were allowed to form for 35 min. The bilayers were rinsed once with TBS, incubated for 5 min with 100 mM NiCl<sub>2</sub> in TBS, rinsed with TBS, and then rinsed with a T cell imaging buffer composed of 1 mM CaCl<sub>2</sub>, 2 mM MgCl<sub>2</sub>, 20 mM HEPES, 137 mM NaCl, 5 mM KCl, 0.7 mM Na<sub>2</sub>HPO<sub>4</sub>, 6 mM d-glucose, and 1% wt/vol bovine serum albumin. Streptavidin (Sigma-Aldrich, St. Louis, MO) was filtered through a 0.1 µm centrifugal filter (EMD Millipore, Billerica, MA) to remove aggregates, diluted with imaging buffer to 0.5 µg/mL, introduced into the flow cells, and incubated for 45 min followed by a rinse with imaging buffer. ICAM-1 and pMHC were washed with TBS using 10,000 MWCO spin concentrators (Vivaspin 500, GE Health Care, Pittsburgh, PA) to remove glycerol storage solution and filtered through a 0.1 µm centrifugal filter (EMD Millipore, Billerica, MA) to remove aggregates. Both proteins were diluted with imaging buffer, introduced into the flow cells, and incubated for 35 min followed by a rinse with imaging buffer. T cells were resuspended in imaging buffer and added to the flow cells 35 min after the final rinse and imaged immediately for 30–60 min. For photobleaching studies of immobilized Atto488-labeled pMHC, coverslips were incubated with 1:10 PLL-g-PEG-Biotin: PLL-g-PEG (SuSoS, Dubendorf, Switzerland) in T cell imaging buffer for 30 minutes, rinsed, and incubated with Streptavidin for 30 minutes. pMHC was diluted with imaging buffer, incubated for 30 minutes followed by a rinse with imaging buffer. All incubations during this protocol were performed at room temperature, and imaging experiments were performed at 37°C.

Jurkat cell experiments were performed on bilayers formed on #1.5 25 mm round coverslips (Warner Instruments, Hamden, CT) in Attofluor cell chambers (Life Technologies, South San Francisco, CA). Prior to experiments, human ICAM-1 was fluorescently labeled with Alexa Fluor 568 NHS Ester Protein Labeling Kit (Life Technologies, South San Francisco, CA). All other imaging chamber and supported lipid bilayer preparation was the same as described before.

## Section 2.6.6: Microscopy

FRAP was performed on a Nikon Eclipse TE-300 inverted fluorescence microscope using a 100X Plan Fluor NA 0.5-1.3 objective (Nikon, Tokyo, Japan). A super high pressure mercury arc lamp (Nikon, Tokyo, Japan) provided illumination for fluorescence images. Images were recorded on a Coolsnap HQ camera (Photometrics, Tuscon, AZ). Metamorph (Molecular Devices, Sunnyvale, CA) and ImageJ software were used to collect, analyze, and process the images.

TIRF experiments were performed on a motorized inverted microscope (Nikon Eclipse Ti-E; Technical Instruments, Burlingame, CA) equipped with a motorized Epi/TIRF illuminator, motorized Intensilight mercury lamp (Nikon C-HGFIE), Perfect Focus system, and a motorized stage (Applied Scientific Instrumentation MS-2000, Eugene, OR). A laser launch with a 488 nm (Coherent OBIS, Santa Clara, CA) diode laser was controlled by an OBIS Scientific Remote (Coherent Inc., Santa Clara, CA) and aligned into a fiber launch custom built by Solamere Technology Group, Inc. (Salt Lake City, UT). Laser powers measured at the sample were 0.6 mW for 250 ms exposures and 6 mW for 30 ms exposures. A dichroic beamsplitter (z488/647rpc; Chroma Technology Corp., Bellows Falls, VT) reflected the laser light through the objective lens (Nikon 1.49 NA TIRF; Technical Instruments, Burlingame, CA) and fluorescence images were recorded using an EM-CCD (iXon 897DU; Andor Inc., South Windsor, CT) after passing through a laser-blocking filter (Z488/647M; Chroma Technology Corp., Bellows Falls, VT). Exposure times, multidimensional acquisitions, and time-lapse periods for all experiments were set using Micro-Manager.<sup>32</sup> A TTL signal from the appropriate laser triggered the camera exposure.

## Section 2.6.7: Data analysis

Analysis of single pMHC:TCR complexes was performed as previously described.<sup>15</sup> Single molecule diffraction-limited spots were detected in raw .tif image stacks of pMHC labeled with MBP-Atto488 or HA-Atto488 molecules by filtering for both size and intensity and linked into tracks using published particle detection and tracking algorithms<sup>18</sup> adapted for MATLAB (The Mathworks; Natick, MA) by Daniel Blair and Eric Dufresne (<http://physics.georgetown.edu/matlab/>; accessed 16 August 2012). Size and intensity thresholds were first determined by eye using a test data set and then applied uniformly to all data collected with the same exposure time and incident laser intensities. Single molecules were identified by step photobleaching detected in an automated way using a Bayesian change point detection algorithm.<sup>19</sup>

## Section 2.7: Chapter 2 references

1. Bell, G. I., Models for the specific adhesion of cells to cells. *Science* **1978**, *200* (4342), 618-627.
2. Zhu, D. M.; Dustin, M. L.; Cairo, C. W.; Golan, D. E., Analysis of two-dimensional dissociation constant of laterally mobile cell adhesion molecules. *Biophys J* **2007**, *92* (3), 1022-34.
3. Huppa, J. B.; Axmann, M.; Mörtelmaier, M. A.; Lillemeier, B. F.; Newell, E. W.; Brameshuber, M.; Klein, L. O.; Schütz, G. J.; Davis, M. M., TCR-peptide-MHC interactions in situ show accelerated kinetics and increased affinity. *Nature* **2010**, *463* (7283), 963-7.
4. Davis, M. M.; Boniface, J. J.; Reich, Z.; Lyons, D.; Hampl, J.; Arden, B.; Chien, Y.-h., Ligand recognition by alpha beta T cell receptors. *Annual Reviews of Immunology* **1998**, *16*, 523-544.
5. Stone, J., D; Chervin, A. S.; Kranz, D. M., T-cell receptor binding affinities and kinetics: impact on T-cell activity and specificity. *Immunology* **2009**, *126*, 165-176.
6. Huang, J.; Zarnitsyna, V. I.; Liu, B.; Edwards, L. J.; Jiang, N.; Evavold, B. D.; Zhu, C., The kinetics of two-dimensional TCR and pMHC interactions determine T-cell responsiveness. *Nature* **2010**, *464* (7290), 932-6.
7. Yin, Y.; Li, Y.; Mariuzza, R. A., Structural basis for self-recognition by autoimmune T-cell receptors. *Immunological Reviews* **2012**, *250*, 32-48.
8. Palmer, E., Negative selection--clearing out the bad apples from the T-cell repertoire. *Nature Reviews Immunology* **2003**, *3*, 383-391.
9. Hemmer, B.; Archelos, J. J.; Hartung, H. P., New concepts in the immunopathogenesis of multiple sclerosis. *Nature Reviews Neuroscience* **2002**, *3* (4), 291-301.
10. Wucherpfennig, K. W.; Sette, A.; Southwood, S.; Oseroff, C.; Matsui, M.; Strominger, J. L.; Hafler, D. A., Structural requirements for binding of an immunodominant myelin basic protein peptide to DR2 isotypes and for its recognition by human T cell clones. **1994**, *179* (1), 279-290.

11. Schubert, D. A.; Gordo, S.; Sabatino, J. J.; Vardhana, S.; Gagnon, E.; Sethi, D. K.; Seth, N. P.; Choudhuri, K.; Reijonen, H.; Nepom, G. T.; Evavold, B. D.; Dustin, M. L.; Wucherpfennig, K. W., Self-reactive human CD4 T cell clones form unusual immunological synapses. *Journal of Experimental Medicine* **2012**, *209* (2), 335-52.
12. Grakoui, A.; Bromley, S. K.; Sumen, C.; Davis, M. M.; Shaw, A. S.; Allen, P. M.; Dustin, M. L., The immunological synapse: a molecular machine controlling T cell activation. *Science* **1999**, *285* (5425), 221-7.
13. Lin, W.-C.; Yu, C.-H.; Triffo, S.; Groves, J. T., Supported membrane formation, characterization, functionalization, and patterning for application in biological science and technology. *Current Protocols in Chemical Biology*, 2010; Vol. 2, pp 235-269.
14. Beckett, D.; Kovaleva, E.; Schatz, P. J., A minimal peptide substrate in biotin holoenzyme synthetase-catalyzed biotinylation. **1999**, *8* (4), 921-929.
15. O'Donoghue, G. P.; Pielak, R. M.; Smoligovets, A. A.; Lin, J. J.; Groves, J. T., Direct single molecule measurement of TCR triggering by agonist pMHC in living primary T cells. *Elife* **2013**, *2*, e00778.
16. Anders, A.-K.; Call, M. J.; Schulze, M.-S. E.; Fowler, K. D.; Schubert, D. A.; Seth, N. P.; Sundberg, E. J.; Wucherpfennig, K. W., HLA-DM captures partially empty HLA-DR molecules for catalyzed removal of peptide. *Nature Immunology* **2011**, *12* (1), 54-61.
17. Coffman, V. C.; Wu, J.-Q., Counting protein molecules using quantitative fluorescence microscopy. *Trends in Biochemical Sciences* **2012**, *37* (11), 499-506.
18. Crocker, J. C.; Grier, D. G., Methods of digital video microscopy for colloidal studies. **1996**, *179*, 298-310.
19. Ensign, D. L.; Pande, V. S., Bayesian detection of intensity changes in single molecule and molecular dynamics trajectories. **2009**, *114* (1), 280-292.
20. Staunton, D.; Marlin, S.; Stratowa, C.; Dustin, M.; Springer, T., Primary structure of ICAM-1 demonstrates interaction between members of the immunoglobulin and integrin supergene families. **1988**, *52* (6), 925-933.
21. Axelrod, D.; Koppel, D.; Schlessinger, J.; Elson, E.; Webb, W., Mobility measurement by analysis of fluorescence photobleaching recovery kinetics. *Biophysical Journal* **1976**, *16*, 1055-1069.

22. Monks, C. R. F.; Freiberg, B. A.; Kupfer, H.; Sciaky, N.; Kupfer, A., Three-dimensional segregation of supramolecular activation clusters in T cells. *Nature* **1998**, *395* (6697), 82-86.
23. Kaizuka, Y.; Douglass, A. D.; Varma, R.; Dustin, M. L.; Vale, R. D., Mechanisms for segregating T cell receptor and adhesion molecules during immunological synapse formation in Jurkat T cells. *2007* *104* (51), 20296-20301.
24. Cole, D. K.; Pumphrey, N. J.; Boulter, J. M.; Sami, M.; Bell, J. I.; Gostick, E.; Price, D. A.; Gao, G. F.; Sewell, A. K.; Jakobsen, B. K., Human TCR-binding affinity is governed by MHC class restriction. *The Journal of Immunology* **2007**, *178*, 5727-5734.
25. van der Merwe, A. P.; Davis, S. J., Molecular interactions mediating T cell antigen recognition. *Annual Review of Immunology* **2003**, *21*, 659-684.
26. Chesla, S. E.; Selvaraj, P.; Zhu, C., Measuring two-dimensional receptor-ligand binding kinetics by micropipette. *Biophysical Journal* **1998**, *75* (3), 1553-1572.
27. Chen, W.; Zarnitsyna, V. I.; Krishna, K. K.; Huang, J.; Zhu, C., Measuring receptor-ligand binding kinetics on cell surfaces: From adhesion frequency to thermal fluctuation methods. *Cellular and Molecular Bioengineering* **2008**, *1* (4), 276-288.
28. Dustin, M. L., Cell adhesion molecules and actin cytoskeleton at immune synapses and kinapses. *Current Opinions in Cell Biology* **2007**, *19* (5), 529-33.
29. Springer, T. A.; Dustin, M. L., Integrin inside-out signaling and the immunological synapse. *Current Opinions in Cell Biology* **2012**, *24* (1), 107-15.
30. Singer, S. J., Intercellular communication and cell-cell adhesion. *Science* **1992**, *255* (5052), 1671-1677.
31. Call, M.; Xing, X.; Cuny, G.; Seth, N.; Altmann, D.; Fugger, L.; Krogsaard, M.; Stein, R.; Wucherpfennig, K., In Vivo Enhancement of Peptide Display by MHC Class II Molecules with Small Molecule Catalysts of Peptide Exchange. **2009**, *182*, 6342-6352.
32. Stuurman, N.; Edelstein, A. D.; Amodaj, N.; Hoover, K. H.; Vale, R. D., Computer control of microscopes using Micro-Manager. **2010**, 1-22.

## Chapter 3

# The Development of a Novel CD80 Supported Membrane Reagent for Single Molecule Investigations of T Cell Signaling

### Section 3.1: Introduction

The CD80 costimulatory protein plays a major role in regulating T cell signal transduction through interactions with its ligands, CD28 and CTLA-4. Our current knowledge of these key molecular binding events primarily comes from *in vitro* solution measurements<sup>1, 2</sup> and bulk *in vivo* imaging studies.<sup>3, 4</sup> We are developing a novel CD80 bilayer reagent for single molecule binding assays in the context of a membrane-membrane juxtacrine signaling interface. This reagent allows us to make the first single molecule observations of CD80 binding its ligand, as well as the first kinetics measurements of this interaction in a membrane environment. Because CD80 is similar in size to pMHC and therefore requires a similar inter-membrane distance in order to bind its ligand,<sup>5</sup> we are also utilizing this reagent to probe changes in the T cell:APC binding interface during TCR triggering.

The novel single molecule CD80 bilayer reagent is a CD80-SNAP-tag fusion protein with a terminal decahistidine tag for attachment to the supported membrane via nickel chelation. The SNAP-tag domain has a single reactive site suitable for the covalent attachment of a bright, photostable fluorophore in a 1:1 stoichiometry.<sup>6, 7</sup> Previous work has shown that CD80 can dimerize<sup>8</sup> and most likely exists as a mixed population of monomers and dimers on the cell surface.<sup>9</sup> To ensure that the fusion protein preserves CD80's oligomeric states and physiological function, we have carefully characterized the new reagent using both traditional biochemical approaches, as well as fluorescence spectroscopy and microscopy techniques.

### Section 3.2: Experimental design

We have created a CD80-SNAP-tag fusion protein as a novel tool for studying T cell signaling in primary mouse T cells. The construct, referred to as CD80-SNAP-His10, consists of the extracellular domain of murine CD80 (residues 1-245), SNAP-tag, and a C-terminal decahistidine (His10) tag (Figure 3.1).<sup>8</sup> SNAP-tag is a mutant of the human DNA repair protein, *O*<sup>6</sup>-alkylguanine-DNA alkyltransferase, which irreversibly transfers

the alkyl group from its substrate,  $O^6$ -alkylguanine-DNA, to one of its cysteine residues. The engineered SNAP-tag protein is optimized to react with  $O^6$ -benzylguanine derivatives, which carry synthetic probes conjugated to their benzene ring. Upon reaction, the substituted benzyl group is transferred to the Cys145 position of SNAP-tag, resulting in a SNAP-tag protein covalently labeled with a synthetic probe, such as an organic fluorophore (Figure 3.2A).<sup>6</sup> This method of fluorescently labeling proteins results in the attachment of the probe to the protein of interest in a 1:1 stoichiometry, which is necessary for single molecule tracking. Compared to other common techniques for fluorophore incorporation in a 1:1 ratio, such as the creation of autofluorescent protein fusions, SNAP-tag fusions offer several key advantages for single molecule studies. First, the synthetic fluorophores used to label the SNAP-tag domain are brighter and more photostable than autofluorescent proteins, leading to higher signal-to-noise ratios and allowing molecules to be tracked over hundreds of seconds. In addition, SNAP-tag fusions can be labeled with benzylguanine fluorophores that display fluorescence emission maxima covering the visible spectrum from 472 to 673 nm, extending the spectral limits set by fluorescent proteins, and providing compatibility with other fluorescently-tagged proteins for multiprotein imaging studies.<sup>10, 11</sup>

```

MACNCQLMQD TPLLKFCPR LILLFVLLIR LSQVSSDVDE QLSKSVKDKV LLPCRYNSPH
EDESEDRIYW QKHKVVLVSV IAGKLVVWPE YKNRTLYDNT TYSLIILGLV LSDRGTYSCV
VQKKERGTYE VKHLALVKLS IKADFSTPNI TESGNPSADT KRITCFASGG FPKPRFSWLE
NGRELPGINT TISQDPESEL YTISSQLDFN TTRNHTIKCL IKYGDHVSE DFTWEKPPED
PPDSKGGSGG SRPAAACRLV MDKDCMKRT TLDSPGKLE LSGCEQGLHR IIFLGKGTSA
ADAVEVPAPA AVLGGPEPLM QATAWLNAYF HQPEAIEEFP VPALHHPVFQ QESFTRQVLW
KLLKVVVFGE VISYSHLAAL AGNPAATAAV KTALSGNPVP ILIPCHRVVQ GDLDVGGYEG
GLAVKEWLLA HEGHRLGKPG LGALEGGSGG SHHHHHHHHH H

```

**Figure 3.1: Amino acid sequence of the CD80 construct.** The fusion protein construct consists of the soluble portion of murine CD80 (pink) fused to SNAP-tag (yellow) with a decahistidine sequence on the C-terminus.

The hybrid live cell-supported membrane junction, in which one cell surface in a juxtacrine signaling system is replaced by a supported lipid bilayer displaying ligands of interest, is a powerful approach for investigating cell-cell signaling.<sup>12, 13, 14</sup> Supported membranes are formed on glass coverslips<sup>15</sup> and functionalized with CD80, pMHC, and ICAM-1. The CD80-SNAP-tag construct is readily attached to a supported membrane via its decahistidine tag. Previous work showed that His10 tags can form essentially irreversible multivalent linkages with nickel-chelating lipids in supported lipid bilayers when assembled using kinetically controlled parameters.<sup>16</sup> MHC and ICAM-1 are also linked to the artificial membrane via nickel chelation. The hybrid live cell-supported membrane setup is illustrated in Figure 3.2B, which shows binding of the SLB proteins to their cognate ligands on the T cell surface. The formation of CD80:ligand complexes is

detected via time-resolved fluorescence microscopy. The protein is imaged at long exposure times (500 ms), at which only the slow moving, bound CD80 molecules can be resolved.<sup>14</sup> In the schematic, CD80 is depicted binding to the covalent homodimer CD28. Studies have suggested that this interaction is monovalent.<sup>17</sup>

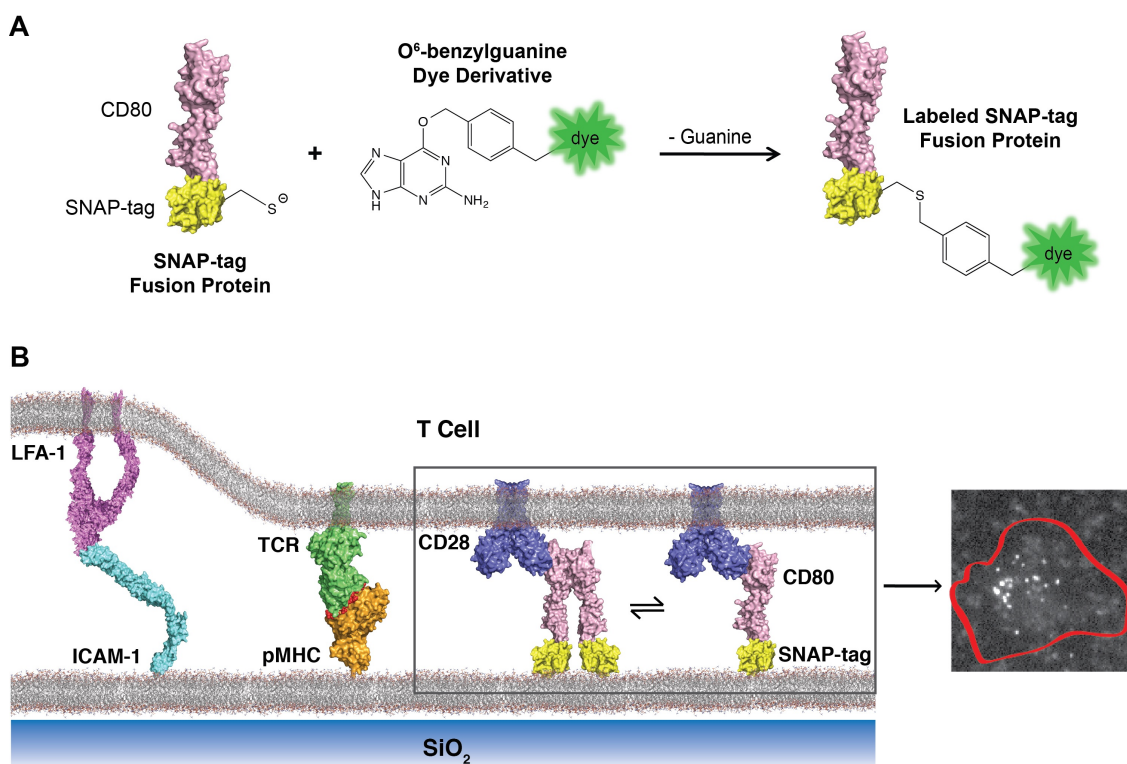


**Figure 3.2: Experimental design.** (A) Schematic showing the SNAP-tag reaction for labeling CD80 with a fluorescent dye molecule. The benzyl group, plus conjugated dye, of the *O*<sup>6</sup>-benzylguanine dye derivative is transferred to the Cys145 site of the SNAP-tag protein, resulting in a CD80 protein labeled with a bright, organic dye in a 1:1 stoichiometry. (B) Schematic of the hybrid live cell-supported membrane system. The CD80-SNAP-His10 construct (PDB, 1DR9, 3KZZ) is shown on a supported lipid bilayer, in both the monomeric and dimeric states. CD80 is shown binding to one of its two ligands, CD28 (PDB, 1YJD). CD80 binding events are observed via single molecule fluorescence microscopy at long exposure times (right). CD80's interactions with its ligands occur in the context of pMHC:TCR binding (PDB, 3QIU), which is aided by integrin adhesion between ICAM-1 (PDB, 1IAM, 1P53) and LFA-1 (PDB, 2K9J).

## Section 3.3: Protein preparation and characterization

### Section 3.3.1: Purification of SNAP-tag proteins

The gene encoding SNAP-tag (SNAP<sub>f</sub>) was cloned into a shuttle vector (pUC57) containing the sequence for the extracellular domain of murine CD80 (residues 1-245)<sup>8</sup> fused to a C-terminal decahistidine tag. The SNAP-tag gene is flanked by a GGSGGS sequence to act as a flexible linker and ensure proper domain folding. The CD80-SNAP-His10 construct was cloned into a pFastbac1 vector and introduced into the bac-to-bac insect cell/baculovirus based expression system according to manufacturer's directions and standard cloning procedures. The protein was secreted from infected ES-sf9 cells and captured on Ni<sup>2+</sup>-nitrilotriacetic acid (NTA) agarose resin. The resin was washed and the protein was eluted using an imidazole gradient. The purified protein was analyzed via gel electrophoresis (SDS-PAGE) to evaluate the purity of the protein.

A SNAP-tag protein construct with a C-terminal decahistidine tag (SNAP-His10) was generated as a control for verifying that the SNAP-tag domain does not perturb the native state of the CD80 protein in the CD80-SNAP-His10 construct. This protein was created by removing the CD80 extracellular domain from the CD80-SNAP-His10 construct through standard cloning procedures and was expressed and purified as described previously.

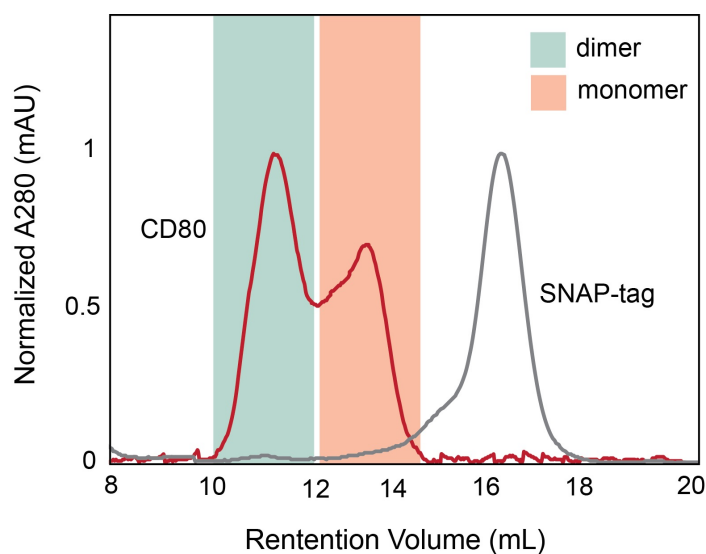


**Figure 3.3: Analytical gel filtration chromatography of SNAP-tag proteins.** Purified CD80-SNAP-His10 and SNAP-His10 were analyzed in solution by gel filtration chromatography. CD80 (22  $\mu$ M) eluted in two peaks, corresponding to dimer and monomer. SNAP-tag (100  $\mu$ M) eluted in a single peak, corresponding to monomeric protein.

The purified SNAP-tag proteins were analyzed in solution using gel filtration chromatography (Figure 3.3). CD80-SNAP-His10 and SNAP-His10 were loaded onto the column at 22  $\mu$ M and 100  $\mu$ M, respectively. CD80 eluted in two peaks, suggesting that the protein forms a mixed population of oligomeric species in solution. The identity of each peak was confirmed by approximating the molecular weight of the corresponding species based on a molecular weight standard curve. The calculated molecular weight of the first CD80 peak is 104 kDa and the molecular weight of the second peak is 30 kDa. The calculated molecular weight of the first peak is very close to the expected molecular weight of a dimer, 101.48 kDa. The second CD80 peak is most likely a monomer, which has an expected molecular weight of 50.74 kDa. Despite the lower observed molecular weight, we do not believe that this peak corresponds to a fragment of the protein, as gel electrophoresis did not reveal any significant bands corresponding to molecular weights below 50 kDa. The discrepancies in molecular weight may be due to overloading the column, which also prevented the two CD80 peaks from being fully resolved into separate peaks. SNAP-tag eluted in a single peak, indicating a single oligomeric species in solution. The calculated molecular weight of this peak is 17 kDa, and is in close agreement with the expected molecular weight of a monomer of the protein, 21.5 kDa.

### **Section 3.3.2: SNAP-tag protein labeling and optimization**

Fluorescence fluctuation spectroscopy and single molecule microscopy studies of CD80 on a supported membrane require it to be labeled with a bright, organic dye in a 1:1 stoichiometry. To achieve this goal, the CD80 protein is covalently labeled with a fluorophore (Alexa Fluor 488, Alexa Fluor 647, or Atto488) on its SNAP-tag domain. The reaction between the SNAP-tag domain and an  $O^6$ -benzylguanine dye derivative is illustrated in Figure 3.2 and results in the transfer of a benzyl dye conjugate to SNAP-tag's Cys145 residue.<sup>7</sup> The activity of the SNAP-tag protein is sensitive to the conditions under which it is expressed, purified, stored, and labeled. Reduced activity results in low labeling efficiencies, which are not ideal for photon counting and single molecule studies. Before performing supported membrane experiments with fluorescently labeled CD80, the activity of SNAP-tag in the CD80-SNAP-His10 construct was carefully optimized in order to preserve maximum SNAP-tag activity and thus achieve maximum labeling efficiency.

Because the extracellular domain of CD80 contains post-translational modifications, such as glycosylation, it was expressed as a secreted protein from a baculovirus/Sf9 insect cell expression system, which is commonly used to express mammalian glycoproteins.<sup>18</sup> During the expression process, the protein is secreted into Sf9 culture at 27 °C until purification of the supernatant. In order to maximize yield, while minimizing degradation and loss of SNAP-tag activity, protein expression and quality was tested every twelve hours between 36 and 108 hours after infecting sf9 cells with baculovirus. At each time point, a sample of supernatant was collected and reacted with an  $O^6$ -benzylguanine Alexa Fluor 647 substrate; the time points were analyzed via gel electrophoresis (SDS-PAGE,

Figure 3.4A). The SDS PAGE analysis reveals fluorescently-labeled protein with a molecular weight around 50 kDa in all samples, corresponding to intact CD80-SNAP-His10. After 48 hours, fluorescently-labeled protein with a molecular weight around 20 kDa begins to appear. This protein is most likely proteolytically-cleaved SNAP-tag domain. Intensity analysis of the gel reveals a peak in intact CD80-SNAP-His10 60 hours after infection, with only minimal cleaved SNAP-tag. All future purifications of the CD80 construct were performed at the 60-hour time point.

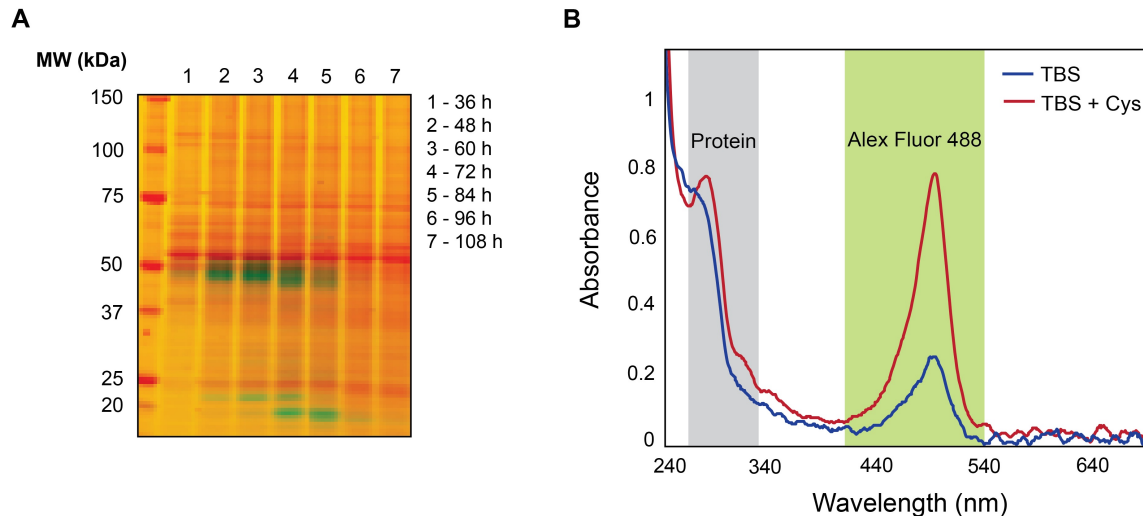


**Figure 3.4: Optimization of SNAP-tag activity in the CD80 fusion protein.** (A) Gel analysis of supernatant collected during the expression of CD80-SNAP-His10. The samples were reacted with an *O*<sup>6</sup>-benzylguanine Alexa Fluor 647 substrate. Ruby-stained protein bands are shown in red and the fluorescently-labeled SNAP-tag bands are shown in green. (B) Uv-vis spectrum of CD80-SNAP-His10 labeled with Alexa Fluor 488 via the SNAP-tag reaction. The blue line corresponds to protein that was purified and labeled in the absence of reducing agent, while the red line corresponds to protein that was purified and labeled under weak reducing conditions (1 mM cysteine).

Oxidation of SNAP-tag's reactive Cys145 will lead to inactivation of the protein.<sup>7</sup> Thus, the activity of the protein is improved in the presence of reducing agents and typical protocols for handling and labeling SNAP-tag fusions suggest adding 1 mM dithiothreitol to all buffers.<sup>6</sup> Analysis of the crystal structure of soluble CD80 reveals two internal disulfide bonds.<sup>8</sup> In order to prevent reduction of these structurally important disulfides, the fusion protein was initially expressed, purified, and labeled in the absence of reducing agents. However, these conditions severely diminish the activity of SNAP-tag and lead to a labeling efficiency of 20-30%. To improve the activity of SNAP-tag, while avoiding reduction of CD80's disulfides, the construct was purified and labeled under weak reducing conditions (1 mM cysteine), leading to an increased labeling efficiency of 90-100%. Figure 3.4B shows a UV-vis spectrum of Alexa Fluor 488-labeled CD80-SNAP-

His10 with (red line) and without (blue line) the addition of cysteine. The labeling efficiencies for the reactions depicted are 92% and 28%, respectively.

### Section 3.3.3: *In vitro* characterization of SNAP-tag proteins on a supported membrane

Following purification and fluorescent labeling, CD80-SNAP-His10 is characterized on a supported membrane to verify conjugation and mobility of the new protein construct. Small unilamellar vesicles (SUVs) consisting of DOPC plus 2% Ni-NTA-DOGS are prepared by sonication. These vesicles are used to form supported membranes on glass and the fluorescently-labeled CD80 fusion protein is attached to the Ni-chelating phospholipids. Coupling of the protein to the bilayer is confirmed by fluorescence spectroscopy (Figure 3.5A, gray circles). To verify that the protein is specifically bound through nickel-histidine interactions, 100 mM EDTA can be added to the bilayer during acquisition of fluorescence measurements (Figure 3.5A, blue circles). EDTA strongly sequesters metal ions, leading to dissociation of any protein bound through nickel-histidine chelation. Loss of fluorescence intensity approximately 40 seconds after the addition of EDTA confirms the specificity of protein attachment, as well as its orientation on the bilayer, with the C-terminal decahistidine tag oriented toward the bilayer and the N-terminal CD80 binding domain oriented away from the bilayer, as depicted in Figure 3.2B.<sup>16, 19</sup>

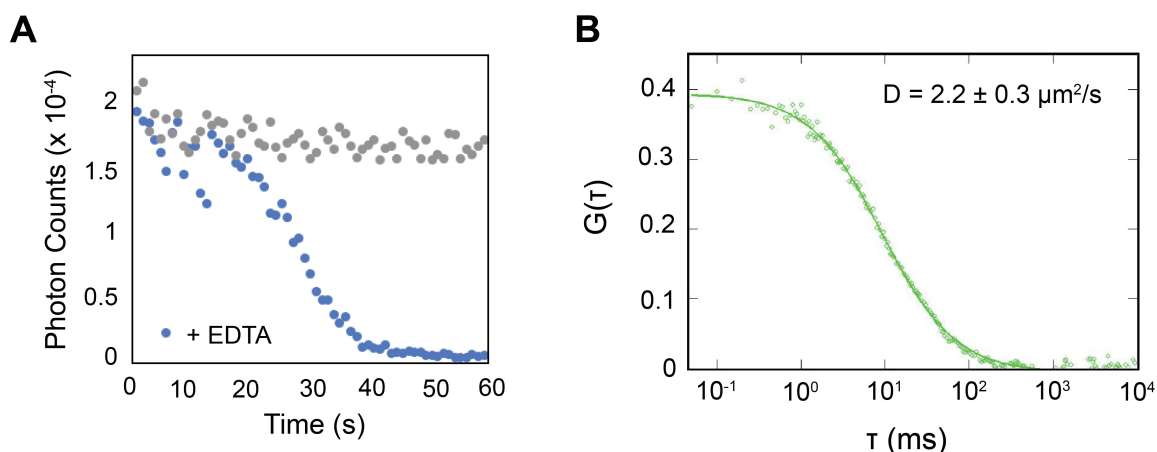


**Figure 3.5: Characterization of CD80-SNAP-His10 on a supported membrane.** (A) Ni-histidine dissociation curve shows that the protein is specifically bound through nickel-histidine interactions and oriented with the N-terminal CD80 binding domain away from the bilayer. (B) FCS is used to characterize the lateral mobility of the protein on a supported lipid bilayer. The plot shows a representative FCS autocorrelation curve, from which the diffusion coefficient is calculated to be  $2.2 \pm 0.3 \mu\text{m}^2/\text{s}$ .

We use fluorescence correlation spectroscopy (FCS) to quantify the lateral mobility of the CD80 construct on a supported membrane. FCS is based on the time-dependent fluctuations in fluorescence intensity as individual molecules pass through the excitation area, a finely-focused, confocal excitation spot. Fluctuations in fluorescence intensity as a function of time,  $\delta F(t)$ , around the average value,  $\langle F(t) \rangle$ , are given by the equation

$$\delta F(t) = F(t) - \langle F(t) \rangle. \quad (3.1)$$

Time traces of fluorescence intensity are correlated with replicas of themselves shifted by different lag times  $\tau$ , resulting in the autocorrelation function,

$$G(\tau) = \frac{\langle \delta F(t) \delta F(t+\tau) \rangle}{\langle F(t) \rangle^2}, \quad (3.2)$$

where  $\delta F(t + \tau)$  is the fluctuation in fluorescence intensity after a lag time  $\tau$ . For a single diffusion species, the data is fitted to an analytical expression of normal two-dimensional diffusion in a two-dimensional Gaussian illumination spot,

$$G(\tau) = \frac{1}{N} \left( \frac{1}{1 + \tau/\tau_D} \right), \quad (3.3)$$

where  $N$  is the average number of molecules in the excitation area and  $\tau_D$  represents the characteristic residence time.<sup>20, 21</sup> Knowing the illumination spot size enables the calculation of the diffusion coefficient,  $D$ , from  $\tau_D$  using the equation,

$$\tau_D = \frac{r^2}{4D}. \quad (3.4)$$

Figure 3.5B shows a representative FCS autocorrelation curve for CD80-SNAP-His10 on a supported lipid bilayer, from which the diffusion coefficient is calculated to be  $2.2 \pm 0.3 \mu\text{m}^2/\text{s}$ . This value is consistent with typical diffusion coefficient ranges of proteins linked to the membrane through polyhistidine-Ni NTA, which are  $\sim 1$  to  $2 \mu\text{m}^2/\text{s}$ .<sup>15</sup>

Next, the oligomerization state of CD80-SNAP-His10 linked to a supported membrane is examined. FCS can be used to identify multiple species in a population only if the mobility of the species differs significantly.<sup>22</sup> Since the CD80 construct is anchored to the membrane, its mobility is dominated by the fluidity of the membrane, not its size.<sup>23</sup> Additionally, the scaling of molecular mobility with size is not well-defined.<sup>24</sup> Due to the complexities associated with using mobility as a readout for cluster size, we turn to photon counting histogram (PCH) spectroscopy<sup>25</sup> and single molecule tracking (SMT) microscopy to determine the oligomeric state of the CD80-SNAP-tag construct on a supported membrane. PCH measures the relative stoichiometries of the fluorescent species in a population, the density of each species, and the relative brightness of each species. However, PCH does not give the absolute number of molecules (fluorescent labels) in each type of oligomer. The absolute stoichiometry can be determined by SMT

in TIRF microscopy by analyzing stepped photobleaching in individually diffusing species.<sup>26</sup>

PCH data acquisition is identical to the FCS technique, in which fluorescent molecules on a supported membrane diffuse through an open confocal spot. The fluorescence intensity fluctuations of labeled CD80-SNAP-His10 molecules yield a super-Poisson (Poi) distribution of photon counts arriving at the detector for a given time interval. The detected photon counts,  $k$ , can be plotted as a histogram and fit to a model in order to determine the average number of molecules in the excitation area and their associated molecular brightness. The probability distribution for  $N$  independent molecules diffusing in an open system is

$$\Pi(k; \bar{N}, B) = \sum_{N=0}^{\infty} P^{(N)}(k; V_0, B) \text{Poi}(N, \bar{N}), \quad (3.5)$$

where  $B$  is the molecular brightness,  $\bar{N}$  is the average number of molecules, and  $V_0$  is the excitation volume. The probability distribution of photon counts for two independent species is given by a convolution of their individual probability distributions,

$$\Pi(k; \bar{N}_1, B_1, \bar{N}_2, B_2) = \Pi(k; \bar{N}_1, B_1) \otimes \Pi(k; \bar{N}_2, B_2), \quad (3.6)$$

where  $\bar{N}_1$  is the average number of species 1,  $\bar{N}_2$  is the average number of species 2,  $B_1$  is the molecular brightness of species 1, and  $B_2$  is the molecular brightness of species 2.<sup>27</sup> We use this two species model to fit data for CD80-SNAP-His10 on a supported membrane, as well as the monomer control, SNAP-His10 (Figure 3.6A). The PCH fitting results of CD80 shown in Figure 3.6A reveal two distinct species that differ in brightness by a factor of  $\sim 2$  ( $2B_2 \cong B_1$ ). Stepped photobleaching analysis of single molecule tracking data demonstrates that the two species are monomers and dimers (Figure 3.6B). To confirm the accuracy of the PCH fit, the data for SNAP-tag, which should be 100% monomeric, is also fit to a two species model. The SNAP-tag fitting results reveal two species with equal brightness, indicating a single oligomeric state in the sample, as expected. The PCH fitting results also provide the average number of molecules for a given species in the excitation area and can be used to determine the relative ratios of each oligomer. At a total surface density of 116 molecules/ $\mu\text{m}^2$ , as determined by quantitative fluorescence,<sup>28</sup> CD80 exists as  $\sim 40\%$  dimer and  $\sim 60\%$  monomer. These results agree with previous reports of CD80 forming a mixed population of monomers and noncovalent dimers on the cell surface.<sup>9</sup>

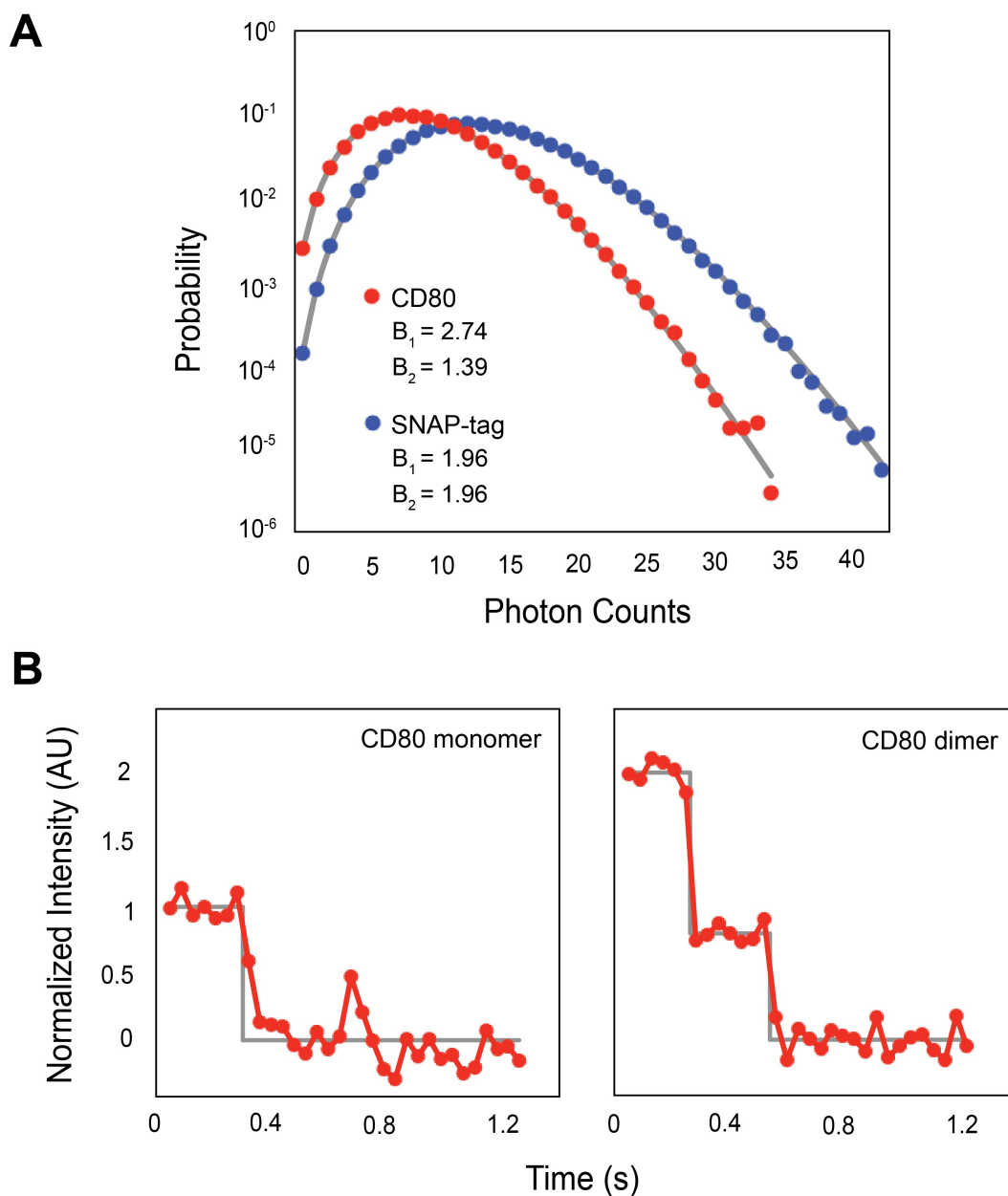


**Figure 3.6: Characterization of CD80 oligomeric state on a supported membrane.**

(A) Representative photon counting histograms for CD80-SNAP-His10 and SNAP-His10 with two-species model data fitting. The molecular brightness ratio  $B_1/B_2$  of CD80 is close to 2. SNAP-tag alone shows only one species because  $B_1 = B_2$ . (B) Representative intensity traces (red) showing a single CD80 monomer (left) and dimer (right) identified by step photobleaching. The single and double step photobleaching events were detected in an automated way using a Bayesian change point detection algorithm (gray). CD80 molecules were tracked using streaming acquisition and a 40 ms exposure time.

### Section 3.3.4: Characterization of CD80 Function

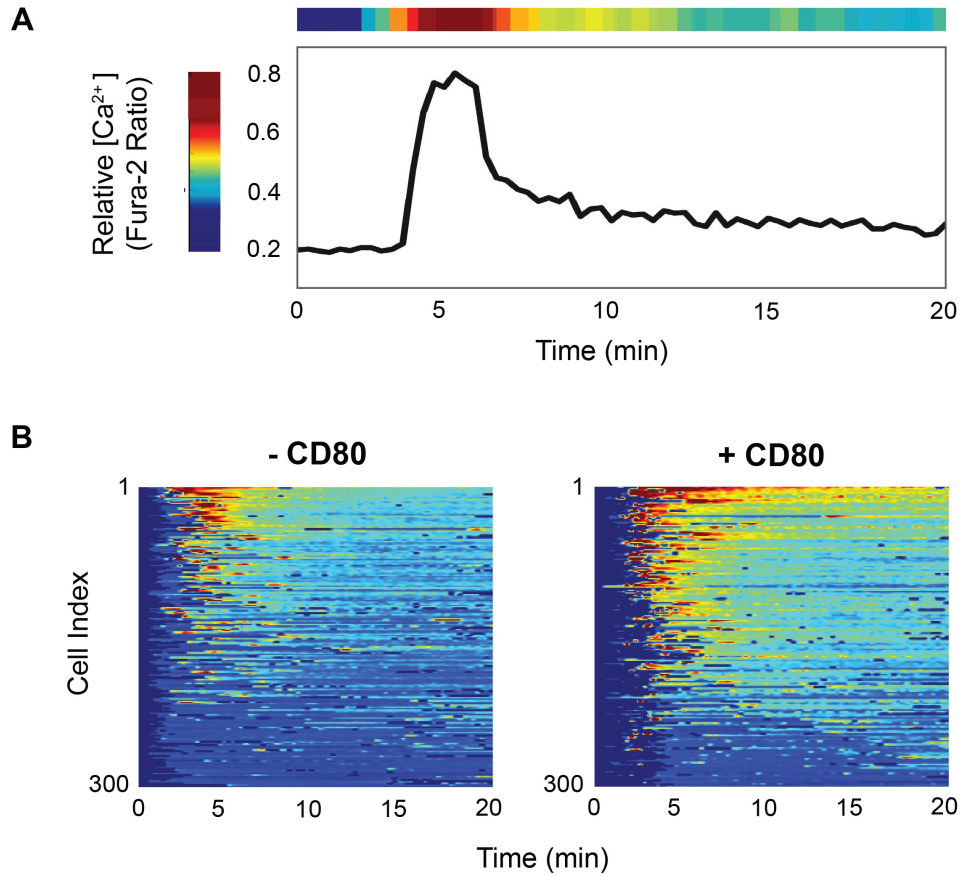


**Figure 3.7: CD80-SNAP-His10 causes increased calcium flux during T cell signaling.**

(A) Calcium trace for a single cell after stimulation. The relative concentration of intracellular calcium is plotted as the 340/380 absorbance ratio of Fura-2. The single cell trace can be represented as a heat map (shown above plot), where red corresponds to the highest calcium concentration and blue to the lowest. (B) Population calcium flux for 300 cells stimulated with and without the CD80-SNAP-tag reagent. Each row of the heat maps corresponds to a single cell. The cells are ordered from highest to lowest peak Fura-2 ratio in the population heat map visualization.

The use of the CD80-SNAP-tag bilayer reagent in cell experiments relies on its ability to elicit costimulatory responses in primary mouse T cells. To investigate T cell triggering with and without CD80-SNAP-His10, we monitor intracellular calcium flux using fluorescence ratio imaging of Fura-2 dye.<sup>12, 29</sup> One of the downstream effects of CD3 phosphorylation during T cell activation is the release of calcium from intracellular stores, which leads to the activation of calcium binding proteins and enzymes that are necessary for the transcription of the IL-2 gene.<sup>29</sup> Thus, examining changes in

intracellular calcium levels is a standard method of monitoring T cell triggering. The CD80 construct is incubated on a supported membrane along with pMHC (MCC-MHC) and ICAM-1, as illustrated in Figure 3.2. Primary mouse T cells are incubated with a membrane permeable derivative of the ratiometric calcium-binding dye Fura-2 (Fura-2-acetoxymethyl) and allowed to interact with the functionalized membrane. Fura-2 absorbs at 340 nm when calcium is bound and 380 nm with no bound calcium; the ratio of 340/380 absorbance can be used to quantify the relative concentration of intracellular calcium in a single cell over time.<sup>30</sup> Figure 3.7A shows the 340/380 absorbance ratio plotted over time for a single cell, which can also be displayed as a heat map (shown above plot). We analyzed a population of 300 cells for each condition (Figure 3.7B) and population calcium flux was integrated over 20 min to include cells responding at different times and provide better signal to noise.<sup>31</sup> The calcium heat maps show a clear increase in the number of cells that flux calcium, as well as the length of sustained calcium flux, for the T cells that are presented with the CD80-SNAP-tag reagent. These results demonstrate that CD80-SNAP-His10 is physiologically functional and capable of costimulating primary mouse T cells.

## **Section 3.4: Monitoring CD80 binding events during TCR triggering**

### **Section 3.4.1: Single molecule observations of CD80 binding its ligand**

The novel CD80-SNAP-tag reagent is used to examine CD80 binding events in primary mouse T cells at the single molecule level. Supported membranes containing fluorescently-labeled CD80, pMHC (MCC-MHC), and ICAM-1 are prepared as previously described. After the addition of T cells, the bilayer is imaged using TIRF microscopy at long exposure time (500 ms) in order to isolate the slow-moving, bound fraction of CD80 molecules (Figure 3.2B, right).<sup>14</sup> To track the binding and unbinding of CD80 to its ligand over time, a sequence of images is recorded using a 3s time lapse. For each frame in a tracking sequence, single molecule diffraction-limited spots are detected by filtering for both size and intensity and linked into tracks using published particle detection and tracking algorithms adapted for MATLAB (Figure 3.8B, blue line).<sup>32</sup> Step photobleaching events are detected in an automated way using a Bayesian change point detection algorithm (Figure 3.8B, gray line).<sup>14, 33</sup>

Stepped photobleaching analysis of single molecule tracking data reveal that the protein is found as a mixed population of monomers and dimers when bound to its ligand. Figure 3.8B shows representative photobleaching traces with one step (left, monomer) and two steps (right, dimer). In order to gain insight into the distribution of oligomeric states in a population of bound CD80 molecules, we constructed a histogram of observed intensities of bound molecules (Figure 3.8A) at two different pMHC densities and constant CD80 density. At a higher pMHC density (0.25 molecules/ $\mu\text{m}^2$ ), the distribution appears to be

bimodal, with peaks centering around  $0.8 \times 10^{-4}$  AU and  $1.3 \times 10^{-4}$  AU. These peaks correspond well to the intensities of monomer and dimer, respectively, as shown in the photobleaching traces. Interestingly, at a lower pMHC density ( $0.05 \text{ molecules}/\mu\text{m}^2$ ), the population shifts to more monomers. A smaller peak is still observed around  $1.4 \times 10^{-4}$  AU (dimer), with a major peak at  $\sim 0.9 \times 10^{-4}$  AU (monomer). Based on these results, we cannot directly quantify the degree of dimerization due to labeling efficiencies  $< 100\%$ . However, we can still conclude that monomers and dimers of bound CD80 are present at both pMHC densities, with an apparent increase in dimerization with pMHC density.

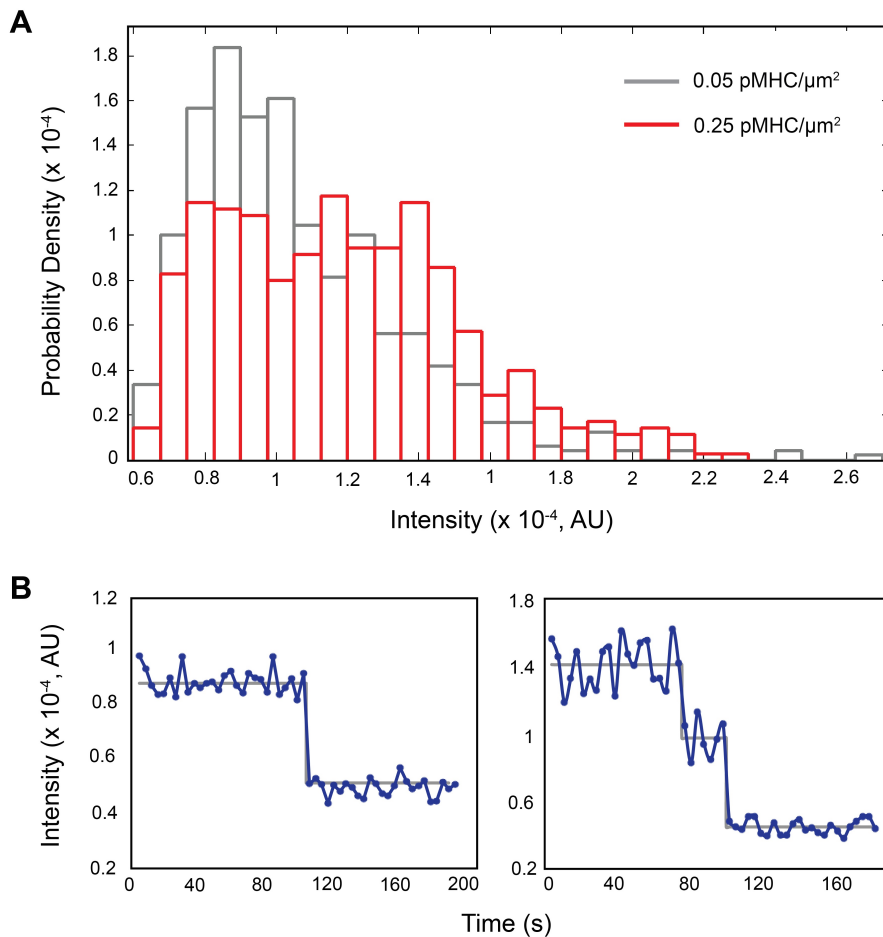


**Figure 3.8: Characterization of bound CD80 oligomeric state.** (A) Intensity histograms of bound CD80 molecules at  $0.05 \text{ pMHC}/\mu\text{m}^2$  (gray) and  $0.25 \text{ pMHC}/\mu\text{m}^2$  (red) densities. (B) Representative intensity traces (blue) showing a single CD80 monomer (left) and dimer (right) identified by step photobleaching. The single and double step photobleaching events were detected in an automated way using a Bayesian change point detection algorithm (gray).

### Section 3.4.2: Single molecule measurements of CD80 dwell time and affinity

We use single molecule tracking to probe the binding kinetics of CD80 while varying pMHC density. Bound CD80 molecules across multiple cell samples are tracked over time, revealing single molecule dwell time distributions at low pMHC density (0.1 molecules/ $\mu\text{m}^2$ ), as well as the optimal density for T cell activation (0.7 molecules/ $\mu\text{m}^2$ ). Figure 3.9A shows the observed dwell time distributions for CD80 binding its ligand at low and optimal pMHC densities. Both distributions are exponential, as expected for molecular binding.<sup>14</sup> Despite the change in CD80 oligomerization with pMHC density, the observed dwell time appears to be constant under the conditions tested. Taking into account the photobleaching time, the mean dwell time,  $\langle\tau_{off}\rangle$ , for CD80 binding its ligand is 8.2 s.

In order to investigate the effect of pMHC density on CD80 affinity, the fraction of bound CD80 molecules at the T cell interface are quantified. For a given cell, we determine the number of bound proteins by imaging at long exposure times and measure the total number of molecules residing in the T cell-supported membrane junction by imaging at short exposure times. The fraction of bound CD80, or binding efficiency, is the ratio of  $\text{CD80}_{\text{bound}}:\text{CD80}_{\text{total}}$ . Figure 3.9B shows histograms of the fraction bound for each condition; each histogram is populated from three replicates using AND CD4+ T cells from three separate mice. The peak fraction bound at low density is  $\sim 0.15$  and increases to  $\sim 0.25$  at optimal density. In addition, a wider range of binding efficiencies is observed at optimal density, between 0 and 100% bound, while no more than 70% bound is observed at the low pMHC density. These results indicate that the affinity of CD80 for its ligand depends on the density of pMHC on the supported membrane and is likely modulated by TCR triggering, as is discussed in the next section.

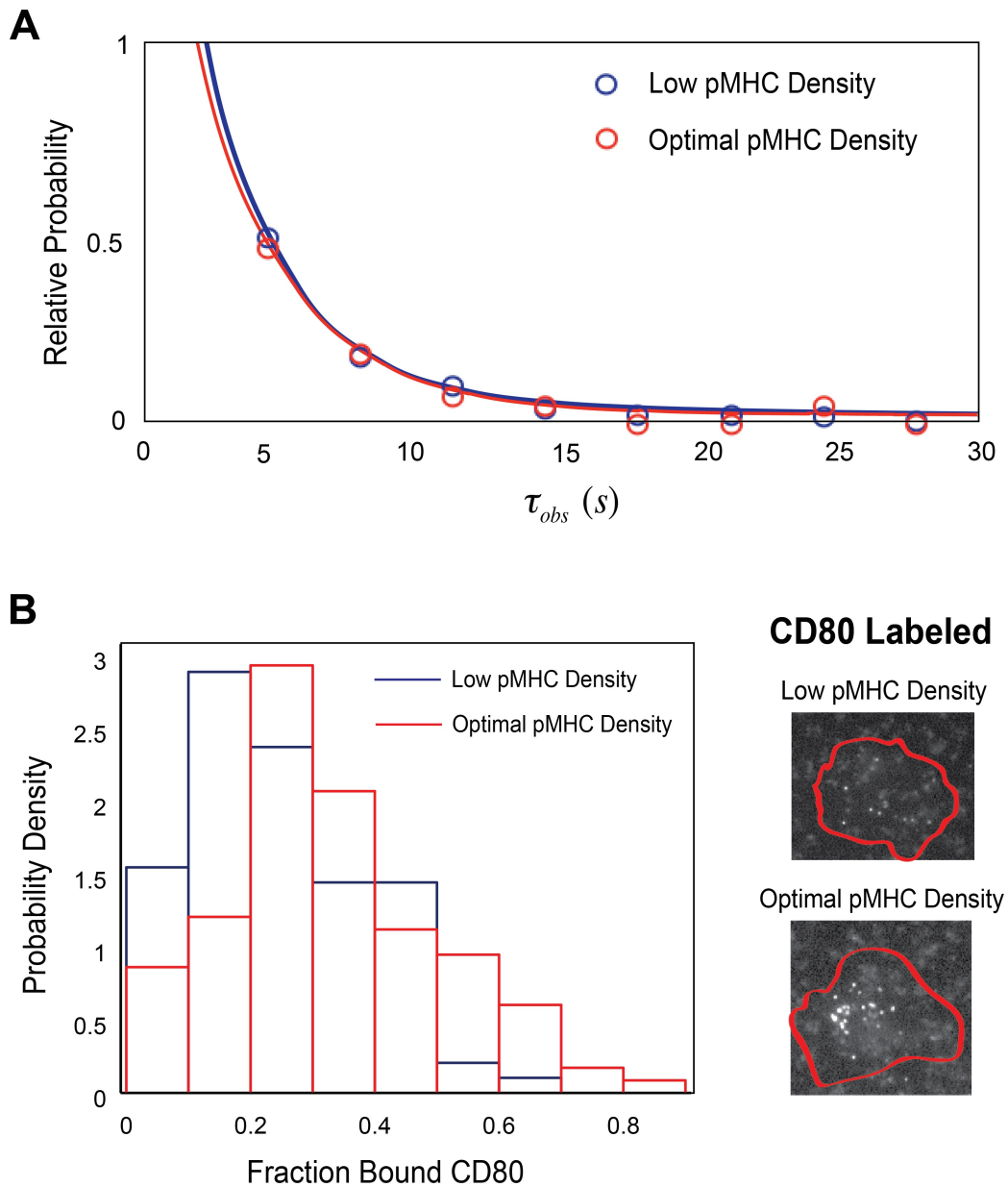


**Figure 3.9: Dwell time and affinity measurements of CD80 binding its ligand. (A)** Observed dwell time distributions ( $\tau_{obs}$ ) for CD80 binding its ligand at low and optimal pMHC density. Dwell times are constant with respect to pMHC density. **(B)** The binding efficiency of CD80 increases at the optimal pMHC density when AND CD4<sup>+</sup> T cell clones are stimulated by the MCC peptide. The optimal pMHC density for MCC is 0.7 molecules/ $\mu\text{m}^2$ . The pMHC low density used is 0.1 molecules/ $\mu\text{m}^2$ .

## Section 3.5: Discussion and conclusions

We have successfully created a novel supported lipid bilayer reagent for single molecule studies of CD80 binding to its ligand during T cell receptor triggering. CD80-SNAP-His10 can be expressed in sf9 insect cells and fluorescently-tagged with a single, bright organic dye with a labeling efficiency greater than 90%. The attachment of the fusion protein to nickel-chelating phospholipids is highly specific and occurs through nickel-histidine interactions. The CD80 reagent is displayed in the correct orientation on the supported membrane, with the C-terminal decahistidine tag oriented toward the bilayer and the N-terminal CD80 binding domain oriented away from the bilayer and ready for interaction with its T cell ligands. Ratiometric calcium imaging demonstrates that the CD80 fusion protein is physiologically functional and capable of inducing increased calcium flux during T cell stimulation.

The CD80-SNAP-tag reagent forms a mixed population of monomers and dimers both in solution and in the membrane environment. CD80 is known to crystalize as a dimer and analytical ultracentrifugation has shown that the protein undergoes noncovalent dimerization in solution with a  $K_D$  in the range of 20-50  $\mu\text{M}$ . Sedimentation velocity boundary analysis showed that monomer and dimer are both present at moderate concentrations and exchange rapidly in solution.<sup>8</sup> These solution results have been verified in the physiologically relevant context of the cell membrane, which could alter the oligomerization state. Photobleaching-based FRET studies have shown that CD80 exists as a mixture of monomers and noncovalent dimers on the cell surface.<sup>9</sup> We used analytical gel filtration chromatography to demonstrate that the CD80-SNAP-His10 fusion protein forms dimers and monomers in solution, as previously described. When conjugated to a supported membrane, the reagent is present as a mixed population of  $\sim 40\%$  dimer and  $\sim 60\%$  monomer, as characterized by photon counting histogram analysis. We verified the presence of monomers and dimers on the membrane via stepped photobleaching analysis of single molecule tracking data.

Single molecule tracking and stepped photobleaching analysis were also used to probe the oligomerization of CD80 bound to its ligand during T cell stimulation with varying densities of pMHC. Monomers and dimers of bound CD80 are present at multiple pMHC densities, with an apparent increase in dimerization with pMHC density. There is some evidence of differential roles of CD80 monomers and dimers during T cell signaling. One model suggests that optimal T cell costimulatory function of CD80 requires high-avidity CD28 engagement by dimeric CD80, followed by dissociation of these noncovalent CD80 dimers, facilitating downregulation of CD28 and internalization of CD80. Thus, dimeric CD80 could be more important for early T cell signaling and its formation may be promoted by pMHC densities above the activation threshold.<sup>4</sup>

We used time-resolved single molecule tracking to determine the molecular binding dwell time of CD80 with its ligand at the membrane-membrane interface. This is the first reported single molecule measurement of CD80 dwell time. Previously, CD80 binding

kinetics have only been measured in solution, using surface plasmon resonance. These studies have shown that CD80 has fast three-dimensional kinetics, binding CD28 for  $\leq 0.6$  s ( $k_{off} \geq 1.6$  s<sup>-1</sup>) and binding CTLA-4 for  $\leq 2$  s ( $k_{off} \geq 0.43$  s<sup>-1</sup>).<sup>2, 34</sup> Our two-dimensional *in situ* kinetics measurements reveal a longer CD80 mean molecular binding dwell time,  $\langle\tau_{off}\rangle$ , of 8.2 s. Because we cannot distinguish CD80 binding to CD28 or CTLA-4, the measured dwell time likely corresponds to a mixture of CD80:CD28 and CD80:CTLA-4 interactions. The discrepancies in molecular unbinding rates between our measurements and the SPR results are likely due to differences in environmental and biological effects on CD80 binding its ligand. At the two-dimensional T cell membrane interface, CD80 binding may be affected by mechanical forces from the membrane, adhesion molecules, and/or the cytoskeleton.<sup>35</sup> Other biological mechanisms induced by T cell signaling, such as a conformational change in the intracellular domain of CD28, could contribute to differences in the *in situ* dwell time.<sup>36, 37</sup> We measured  $\langle\tau_{off}\rangle$  at two different densities of pMHC on the supported membrane surface, including a low density and the optimal density required for T cell triggering. The measured molecular binding dwell time is constant with changing pMHC density.

By directly monitoring individual CD80 binding events, we observe an increase in CD80 binding efficiency at the optimal pMHC:TCR density. Since  $\langle\tau_{off}\rangle$  is constant with pMHC density and  $k_{on}$  is a contextual parameter that is intrinsically affected by the intermembrane environment,<sup>38</sup> our results indicate that the affinity modulation of CD80:ligand binding is mediated by a change in  $k_{on}$  that is regulated by environmental changes due to TCR triggering. We postulate that the modulation of the binding interface is caused by pMHC:TCR feedback after the first few molecular interactions occur. One potential mechanism to explain this phenomenon is that TCR signaling could induce a structural change to the intracellular domain of CD28 that also contributes to an increase in the CD80  $k_{on}$ .<sup>36, 37</sup> These results suggest that membrane-proximal feedback through the TCR may amplify costimulatory signals by increasing the efficiency of costimulatory receptor binding.

## Section 3.6: Materials and methods

### Section 3.6.1: Protein expression, purification, and labeling

Bi-hexahistidine-tagged major histocompatibility complex (MHC) class II I-Ek protein and decahistidine-tagged ICAM-1 were produced and purified as previously described.<sup>16</sup> A plasmid containing CD80 fused to decahistidine-tagged SNAP<sub>F</sub> (GenScript, Piscataway, NJ) was subcloned into a pFastBac1 vector (Life Technologies, Carlsbad, CA). A second plasmid containing SNAP<sub>F</sub> fused to a decahistidine tag was generated by standard cloning procedures and subcloned into a pFastBac1 vector. Both proteins were expressed in ES-sf9 cells and purified by Ni<sup>2+</sup>-nitrilotriacetic acid (NTA) agarose affinity (Qiagen, Venlo, Netherlands) with 1mM cysteine. For gel filtration analysis of the

purified proteins, CD80-SNAP-His10 and SNAP-His10 were filtered through a 0.22  $\mu\text{m}$  filter and injected on a Superdex 200 size exclusion column using an AKTA explorer 100 FPLC system (Amersham Pharmacia Biotech, Piscataway, NJ).

SNAP-tag proteins were labeled with a four-fold molar excess of SNAP-Surface 488 (New England BioLabs, Ipswich, MA). Excess dye was removed using a 10k molecular weight cutoff Vivaspin centrifugal concentrator (GE Healthcare, Little Chalfont, UK) and the labeling efficiency was determined via UV-vis (Nanodrop 2000 Spectrophotometer; Thermo Scientific, Waltham, MA).

### **Section 3.6.2: Cell culture**

AND CD4<sup>+</sup> T cell blasts<sup>39</sup> were cultured from the lymph nodes and spleens of first generation ANDxB10.BR mice in accordance with Lawrence Berkeley National Laboratory Animal Welfare and Research Committee approved protocol 17702. Cells were maintained in Dulbecco's Modified Eagle's Medium (Life Technologies, Carlsbad, CA) supplemented with 10% defined FBS (HyClone), 1 mM sodium pyruvate, 2 mM L-glutamine, 100  $\mu\text{M}$  nonessential amino acids, 100  $\mu\text{M}$  essential amino acids, 50 mM sodium bicarbonate, 50  $\mu\text{M}$  2-mercaptoethanol, 100 units/mL penicillin, and 100  $\mu\text{g}/\text{mL}$  streptomycin (all Life Technologies, Carlsbad, CA). The cells were stimulated with 2  $\mu\text{M}$  moth cytochrome c (amino acids 88-103) peptide immediately after harvest. At 24 h after harvest (day 2), 50 U/mL mouse recombinant IL-2 (Roche Applied Science Inc., Indianapolis, IN) was added to the T-cell medium. IL-2 was added every 48 hours and cells were used for calcium imaging on day 5 or 7.<sup>13, 40</sup>

### **Section 3.6.3: Imaging chamber and supported lipid bilayer preparation**

For *in vitro* membrane characterization experiments, small unilamellar vesicles (SUVs) were formed by tip sonication or extrusion of a solution composed of 98 mol % 1,2-dioleoyl-sn-glycero-3-phosphocholine (DOPC) and 2 mol % 1,2 dioleoyl-sn-glycero-3-[(N-(5-amino-1-carboxypentyl) iminodiacetic acid) succinyl] (nickel salt) (Ni-NTA-DOGS) (Avanti Polar Lipids, Alabaster, AL) in Milli-Q water (EMD Millipore, Billerica, MA). Prior to experiments, #1.5 25 mm round coverslips (Warner Instruments, Hamden, CT) were ultrasonicated for 30 min in 50:50 isopropyl alcohol:water, rinsed thoroughly in Milli-Q water (EMD Millipore, Billerica, MA), etched for 5 min in piranha solution (3:1 sulfuric acid:hydrogen peroxide), and again rinsed thoroughly in Milli-Q water. The coverslips were used in the assembly of Atof fluor cell chambers (Life Technologies, South San Francisco, CA). SUVs were deposited onto the glass coverslips and bilayers were allowed to form for 35 min. The bilayers were rinsed once with TBS, incubated for 5 min with 100 mM NiCl<sub>2</sub> in TBS, rinsed with TBS, and then rinsed with imaging buffer. Fluorescently labeled CD80-SNAP-His10 or SNAP-His10 was diluted with imaging

buffer, introduced into the imaging chambers, and incubated for 35 min followed by a rinse with imaging buffer.

For cell experiments, bilayers were formed in FCS2 Closed Chamber Systems (flow cells; Bioptechs, Butler, PA), as described in Chapter 2. 48 hr prior to experiments, murine MHC was loaded with peptide (MCC) at 37 °C in a buffer composed of 1% wt/vol bovine serum albumin in phosphate buffered saline and brought to pH 4.5 with citric acid. Unbound peptide was separated from peptide loaded MHC (pMHC) using 10k molecular weight cutoff Vivaspin centrifugal concentrators (GE Healthcare, Little Chalfont, UK). pMHC, ICAM-1, and CD80-SNAP-His10 were diluted with imaging buffer, introduced into the flow cells, and incubated for 35 min followed by a rinse with imaging buffer. Cells were resuspended in imaging buffer and added to the bilayer. Experiments were performed at 37 °C. For calcium imaging experiments, cells were loaded with 1 μM Fura-2-AM (acetoxymethyl) (Life Technologies, Carlsbad, CA) for 15 min in cell media without FBS at room temperature, washed, incubated for additional 20 min in serum rich media at 37 °C, and resuspended in imaging buffer before injection.

### **Section 3.6.4: Spectroscopy and microscopy**

FCS experiments were conducted with a home-built setup. An Eclipse TE2000-E microscope (Nikon Tokyo, Japan) was used and the illumination for the fluorescently-labeled protein was provided using an 488 nm Kr-Argon ion laser (Newport Corp., Irvine, CA). A custom-built confocal system equipped with hardware correlator (Correlator.com, Bridgewater, NJ) was used for FCS measurements. The confocal volume was calibrated by 100 nM fluorescein in 1M NaOH solution. The autocorrelation functions were fitted to a simple, one-component, 2-dimensional model and the diffusion constant was back calculated from the calibrated confocal volume following published methods.<sup>41</sup> MATLAB (The Mathworks, Natick, MA) was used to analyze the autocorrelation function. Photon counting measurements were done using the same setup but the analysis followed standard methods.<sup>27, 25</sup> The PCH data were analyzed using the Globals software package (Laboratory for Fluorescence Dynamics, Urbana Champaign, IL). The nickel dissociation curve was acquired using the same fluorescence fluctuation spectroscopy setup. A CD80-SNAP-His10 bilayer was rinsed with 1x TBS and photon counts were detected over time, with and without the addition of 100 mM EDTA.

For calcium imaging, emission at 510 nm was collected after excitation at 340 and 380 nm via 40x S Fluor Objective (Nikon Tokyo, Japan) on a CoolSnap K4 (Roper Scientific) camera on a TE2000-E (Nikon Tokyo, Japan) microscope with Metamorph (Molecular Devices, Sunnyvale, CA) imaging software. Analysis of ratio and population means was done in MATLAB (The Mathworks, Natick, MA). Increase in Fura-2 ratio above basal level for each cell was integrated for the imaging period of 20 min.

TIRF experiments were performed on a motorized inverted microscope (Nikon Eclipse Ti-E; Technical Instruments, Burlingame, CA) equipped with a motorized Epi/TIRF illuminator, motorized Intensilight mercury lamp (Nikon C-HGFIE), Perfect Focus system, and a motorized stage (Applied Scientific Instrumentation MS-2000, Eugene, OR). A laser launch with a 488 nm (Coherent OBIS, Santa Clara, CA) diode laser was controlled by an OBIS Scientific Remote (Coherent Inc., Santa Clara, CA) and aligned into a fiber launch custom built by Solamere Technology Group, Inc. (Salt Lake City, UT). Laser powers measured at the sample were 0.6 mW for 250 ms exposures and 6 mW for 30 ms exposures. A dichroic beamsplitter (z488/647rpc; Chroma Technology Corp., Bellows Falls, VT) reflected the laser light through the objective lens (Nikon 1.49 NA TIRF; Technical Instruments, Burlingame, CA) and fluorescence images were recorded using an EM-CCD (iXon 897DU; Andor Inc., South Windsor, CT) after passing through a laser-blocking filter (Z488/647M; Chroma Technology Corp., Bellows Falls, VT). Exposure times, multidimensional acquisitions, and time-lapse periods for all experiments were set using Micro-Manager. A TTL signal from the appropriate laser triggered the camera exposure. Single molecule analysis of bound CD80 was performed as described in Chapter 2.

### **Section 3.7: Chapter 3 references**

1. Linsley, P. S.; Greene, J. L.; Brady, W.; Bajorath, J.; Ledbetter, J. A.; Peach, R., Human B7-1 (CD80) and B7-2 (CD86) bind with similar avidities but distinct kinetics to CD28 and CTLA-4 receptors. *Immunity* **1994**, *1* (9), 793-801.
2. van der Merwe, P. A.; Bodian, D. L.; Daenke, S.; Linsley, P.; Davis, S. J., CD80 (B7-1) Binds Both CD28 and CTLA-4 with a Low Affinity and Very Fast Kinetics *The Journal of Experimental Medicine* **1997**, *185* (3), 393-403.
3. Yokosuka, T.; Kobayashi, W.; Sakata-Sogawa, K.; Takamatsu, M.; Hashimoto-Tane, A.; Dustin, M. L.; Tokunaga, M.; Saito, T., Spatiotemporal regulation of T cell costimulation by TCR-CD28 microclusters and protein kinase C theta translocation. *Immunity* **2008**, *29* (4), 589-601.
4. Bhatia, S.; Sun, K.; Almo, S. C.; Nathenson, S. G.; Hodes, R. J., Dynamic Equilibrium of B7-1 Dimers and Monomers Differentially Affects Immunological Synapse Formation and T Cell Activation in Response to TCR/CD28 Stimulation. *The Journal of Immunology* **2010**, *184*, 1821-1828.
5. Sharpe, A. H.; Freeman, G. J., The B7-CD28 superfamily. *Nature Reviews Immunology* **2002**, *2* (2), 116-126.

6. Keppler, A.; Gendreizig, S.; Gronemeyer, T.; Pick, H.; Vogel, H.; Johnsson, K., A general method for the covalent labeling of fusion proteins with small molecules *in vivo*. *Nature Biotechnology* **2002**, *21*, 86-89.
7. Keppler, A.; Kindermann, M.; Gendreizig, S.; Pick, H.; Vogel, H.; Johnsson, K., Labeling of fusion proteins of O6-alkylguanine-DNA alkyltransferase with small molecules in vivo and in vitro. *Methods* **2004**, *32*, 437-444.
8. Ikemizu, S.; Gilbert, R. J.; Fennelly, J. A.; Collins, A. V.; Harlos, K.; Jones, E. Y.; Stuart, D. I.; Davis, S. J., Structure and dimerization of a soluble form of B7-1. *Immunity* **2000**, *12* (1), 51-60.
9. Bhatia, S.; Edidin, M.; Almo, S. C.; Nathenson, S. G., Different cell surface oligomeric states of B7-1 and B7-2: implications for signaling. *Proceedings of the National Academy of Science* **2005**, *102* (43), 15569-15574.
10. Johnsson, K., Visualizing biochemical activities in living cells. *Nature Chemical Biology* **2009**, *5* (2), 63-65.
11. Keppler, A.; Arrivoli, C.; Sironi, L.; Ellenberg, J., Fluorophores for live cell imaging of AGT fusion proteins across the visible spectrum. *Biotechniques* **2006**, *41* (2), 167-175.
12. Grakoui, A.; Bromley, S. K.; Sumen, C.; Davis, M. M.; Shaw, A. S.; Allen, P. M.; Dustin, M. L., The immunological synapse: a molecular machine controlling T cell activation. *Science* **1999**, *285* (5425), 221-7.
13. Mossman, K. D.; Campi, G.; Groves, J. T.; Dustin, M. L., Altered TCR signaling from geometrically repatterned immunological synapses. *Science* **2005**, *310* (5751), 1191-1193.
14. O'Donoghue, G. P.; Pielak, R. M.; Smoligovets, A. A.; Lin, J. J.; Groves, J. T., Direct single molecule measurement of TCR triggering by agonist pMHC in living primary T cells. *Elife* **2013**, *2*, e00778.
15. Lin, W.-C.; Yu, C.-H.; Triffo, S.; Groves, J. T., Supported membrane formation, characterization, functionalization, and patterning for application in biological science and technology. **2010**, *2*, 235-269.
16. Nye, J. A.; Groves, J. T., Kinetic control of histidine-tagged protein surface density on supported lipid bilayers. *Langmuir* **2008**, *24* (8), 4145-4149.
17. Evans, E. J.; Esnouf, R. M.; Manso-Sancho, R.; Gilbert, R. J. C.; James, J. R.; Yu, C.; Fennelly, J. A.; Vowles, C.; Hanke, T.; Walse, B.; Hunig, T.; Sorenson, P.; Stuart, D.

- I.; Davis, S. J., Crystal structure of a soluble CD28-Fab complex. *Nature Immunology* **2005**, *6*, 271-279.
18. Nettleship, J. E.; Assenberg, R.; Diprose, J. M.; Rahman-Huq, N.; Owens, R. J., Recent advances in the production of proteins in insect and mammalian cells for structural biology. *Journal of Structural Biology* **2010**, *172*, 55-65.
19. Xu, Q.; Lin, W.-C.; Petit, R. S.; Groves, J. T., EphA2 Receptor Activation by Monomeric Ephrin-A1 on Supported Membranes. *Biophysical Journal* **2011**, *101*, 2731-2739.
20. Enderlein, J.; Gregor, I.; Patra, D.; Dertinger, T.; Kaupp, U. B., Performance of fluorescence correlation spectroscopy for measuring diffusion and concentration. *ChemPhysChem* **2005**, *6*, 2324-2336.
21. Groves, J. T.; Parthasarathy, R.; Forstner, M. B., Fluorescence imaging of membrane dynamics. *Annual Review of Biomedical Engineering* **2008**, *10*, 311-338.
22. Meseth, U.; Wohland, T.; Rigler, R.; Vogel, H., Resolution of fluorescence correlation measurements. *Biophysical Journal* **1999**, *76*, 1619-1631.
23. Saffman, P.; Delbruck, M., Brownian motion in biological membranes. *Proceedings of the National Academy of Sciences* **1975**, *72* (8), 3111-3113.
24. Naji, A.; Levine, A. J.; Pincus, P., Corrections to the Saffman-Delbrück mobility for membrane bound proteins. *Biophysical Journal: Biophysical Letters* **2007**, *93* (11), L49-L51.
25. Muller, J. D.; Chen, Y.; Gratton, E., Resolving heterogeneity on the single molecular level with the photon-counting histogram. *Biophysical Journal* **2000**, *78*, 474-486.
26. Lin, W.-C.; Iversen, L.; Tu, H.-L.; Rhodes, C.; Christensen, S. M.; Iwig, J. S.; Hansen, S. D.; Huang, W. Y.; Groves, J. T., H-Ras forms dimers on membrane surfaces via a protein-protein interface. *Proceedings of the National Academy of Sciences* **2014**, *111* (8), 2996-3001.
27. Chen, Y.; Muller, J. D.; So, P. T.; Gratton, E., The photon counting histogram in fluorescence fluctuation spectroscopy. *Biophysical Journal* **1999**, *77*, 553-567.
28. Galush, W. J.; Nye, J. A.; Groves, J. T., Quantitative fluorescence microscopy using supported lipid bilayer standards. *Biophysical Journal* **2008**, *95*, 2512-2519.

29. Wulfing, C.; Rabinowitz, J. D.; Beeson, C.; Sjaastad, M. D.; McConnell, H. M.; Davis, M. M., Kinetics and extent of T cell activation as measured with the calcium signal. *The Journal of Experimental Medicine* **1997**, *185* (10), 1815-1825.
30. Tsien, R. Y.; Rink, T. J.; Poenie, M., Measurement of cytosolic free Ca<sup>2+</sup> in individual small cells using fluorescence microscopy with dual excitation wavelengths. *Cell Calcium* **1985**, *6*, 145-157.
31. Manz, B. N.; Jackson, B. L.; Petit, R. S.; Dustin, M. L.; Groves, J. T., T-cell triggering thresholds are modulated by the number of antigen within individual T-cell receptor clusters. *Proceedings of the National Academy of Science* **2011**, *108* (22), 9089-9094.
32. Crocker, J. C.; Grier, D. G., Methods of digital video microscopy for colloidal studies. **1996**, *179*, 298-310.
33. Ensign, D. L.; Pande, V. S., Bayesian detection of intensity changes in single molecule and molecular dynamics trajectories. **2009**, *114* (1), 280-292.
34. Collins, A. V.; Brodie, D. W.; Gilbert, R. J. C.; Iaboni, A.; Manso-Sancho, R.; Walse, B.; Stuart, D. I.; van der Merwe, P. A.; Davis, S. J., The interaction properties of costimulatory molecules revisited. *Immunity* **2002**, *17* (201-210).
35. Zarnitsyna, V.; Zhu, C., T cell triggering: insights from 2D kinetics analysis of molecular interactions. *Physical Biology* **2012**, *9* (045005).
36. Sanchez-Lockhart, M.; Kim, M.; Miller, J., Cutting edge: A role for inside-out signaling in TCR regulation of CD28 ligand binding. *The Journal of Immunology* **2011**, *187*, 5515-5519.
37. Sanchez-Lockhart, M.; Rojas, A. V.; Fettis, M. M.; Bauserman, R.; Higa, T. R.; Miao, H.; Waugh, R. E.; Miller, J., T cell receptor signaling can directly enhance the avidity of CD28 ligand binding. *PLoS One* **2014**, *9* (e89263).
38. Hu, J.; Lipowsky, R.; Weikl, T. R., Binding constants of membrane-anchored receptors and ligands depend strongly on the nanoscale roughness of membranes. *Proceedings of the National Academy of Science* **2013**, *110* (38), 15283–15288.
39. Kaye, J.; Hsu, M.-L.; Sauron, M.-E.; Jameson, S. C.; Gascoigne, N. R.; Hedrick, S. M., Selective development of CD4<sup>+</sup> T cells in transgenic mice expressing a class II MHC-restricted antigen receptor *Nature* **1989**, *341*, 746-749.
40. Manz, B.; Jackson, B. L.; Petit, R. S.; Dustin, M. L.; Groves, J. T., T-cell triggering thresholds are modulated by the number of antigen within individual T-cell

receptor clusters. *Proceedings of the National Academy of Science* **2011**, *108* (22), 9089-9094.

41. Haustein, E.; Schwille, P., Fluorescence correlation spectroscopy: novel variations of an established technique. *Annual Review of Biophysics and Biomolecular Structure* **2007**, *36*, 151-169.

## Chapter 4

# Probing pMHC:TCR Binding Thresholds for T cell Activation

### Section 4.1: Introduction

T cells can detect very few high-affinity foreign antigen-MHC complexes in the presence of abundant low affinity self-pMHC molecules.<sup>1</sup> The interaction between TCR and stimulating, foreign antigen-MHC triggers the receptor and leads to downstream cellular activation. Despite its role in initiating the adaptive immune response and protecting the host against invading pathogens, the mechanism of T cell activation is still largely unknown. Several theories have suggested that T cell receptor occupancy, either the number of occupied TCRs<sup>2</sup> or the length of occupancy (dwell time),<sup>3, 4</sup> is the basis of antigen discrimination.<sup>5</sup> We are interested in measuring these physical binding parameters and directly correlating them with activation in a single cell in order to understand the minimum input required for a T cell to activate.

In order to measure all of the pMHC:TCR interactions leading to T cell activation, we have developed a novel method to simultaneously observe membrane surface receptor:ligand binding and cellular activation in a single living primary mouse T cell. Using single molecule TIRF microscopy, we can detect every pMHC:TCR complex in a single cell and quantify the cumulative number of molecular binding events and associated dwell times. TIRF imaging can be alternated with epifluorescence imaging of NFAT-mCherry in the T cell and NFAT subcellular localization can be used as a digital readout of activation. NFAT, or nuclear factor of activated T cells, is a transcription factor that is translocated to the nucleus during T cell signaling, leading to the transcription of the cytokine IL-2.<sup>6</sup> An NFAT-autofluorescent protein fusion has previously been shown to be an unambiguous readout for productive TCR signaling in individual cells.<sup>7</sup>

In this study, we use the mouse MHC class II protein, I-E<sup>k</sup>, loaded with either the strong agonist MCC or weak agonist T102S to trigger TCR.<sup>8, 9</sup> By comparing the activation threshold for a strong and weak agonist, we can gain further insight into the mechanism of antigen discrimination.

## Section 4.2: Experimental design

### Section 4.2.1: Hybrid live cell-artificial membrane system

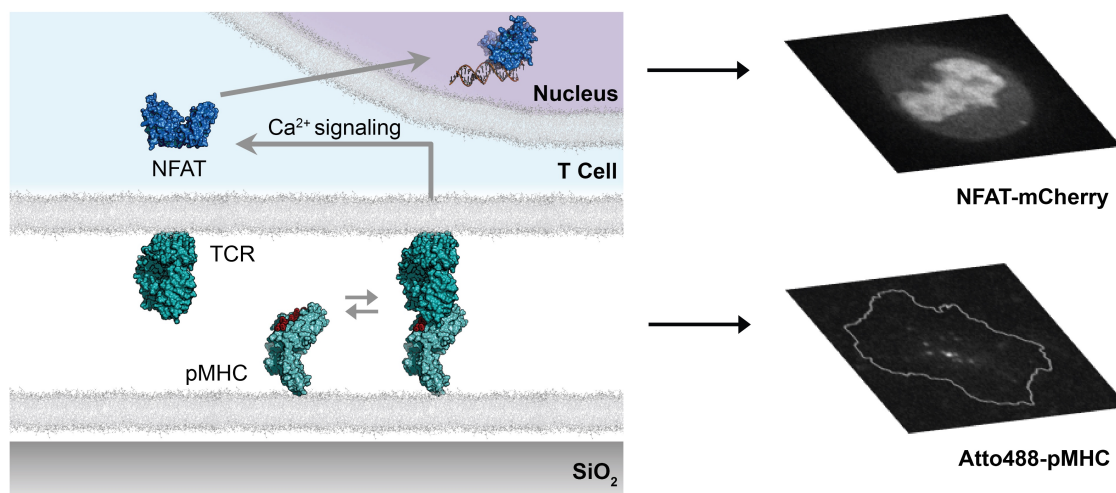


**Figure 4.1: Experimental setup for the simultaneous observation of pMHC:TCR binding and NFAT nuclear translocation in living T cells.** The schematic shows Atto488-pMHC binding to TCR, which can be visualized using single molecule TIRF microscopy (bottom right image). Binding events trigger an influx of calcium in the T cell cytosol, which eventually leads to the nuclear translocation of the transcription factor NFAT. This translocation event is recorded by imaging NFAT-mCherry using epifluorescence microscopy (top right image).

We have designed a novel supported membrane-cell system for the simultaneous detection of cell surface binding events and downstream cellular activation in a single primary mouse T cell (Figure 4.1). The supported membrane is functionalized with MHC (IE<sup>k</sup>) and ICAM-1, both linked to the membrane via C-terminal poly-His tag binding to Ni-chelating lipids.<sup>10</sup> MHC is loaded with peptide (MCC or T102S), which is covalently labeled with the photostable fluorophore Atto488 using maleimide-thiol chemistry.<sup>11</sup> After contact between the T cell and the supported membrane, individual pMHC:TCR complexes are detected by single molecule TIRF microscopy at long exposure times (500 ms), at which only the slow moving, bound pMHC molecules can be resolved (Figure 4.1, bottom right image).<sup>11</sup> The use of singly-labeled peptide in combination with the described imaging technique allows us to directly measure the number of pMHC:TCR binding events and the observed dwell time,  $\tau_{obs}$ , associated with each binding event in a single cell.

AND CD4<sup>+</sup> T cell clones are transduced with NFAT-mCherry in order to monitor NFAT nucleoplasmic shuttling, which occurs in activated T cells.<sup>7</sup> The binding of pMHC on the

supported bilayer to TCR on the cell may result in changes in the localization of NFAT-mCherry, which is detected via epifluorescence microscopy (Figure 4.1, top right image). The use of the NFAT-fluorescent protein fusion and epifluorescence imaging allows us to directly probe the activation state of a single T cell.

### Section 4.2.2: NFAT Translocation Assay

Detection of NFAT localization is a powerful method for measuring T cell activation on a single cell level. Because NFAT translocates to the nucleus in response to sustained calcium release during T cell signal transduction, epifluorescence microscopy imaging of NFAT subcellular localization provides a clear, ratiometric imaging output of individual T cell responses to stimulation.<sup>7</sup> The NFAT translocation assay has several advantages over traditional readouts of T cell activation, such as IL-2 release and intracellular calcium flux. Because the production of the cytokine IL-2 marks a commitment of the T cell to proliferation, it has often been used as a reliable readout of potent T cell activation. However, maximal intracellular accumulation of the protein *in vivo* can take as long as 12 to 14 hours and occurs in less than 50% of cells in a population.<sup>12</sup> While recent single cell measurements of IL-2 secretion have been reported,<sup>13</sup> examination of IL-2 release is mostly performed on the population level, making it difficult to correlate the pMHC:TCR binding in a single cell to its downstream signaling response. Although intracellular calcium flux can be observed as early as 6-7 seconds after stimulation,<sup>14</sup> and allows for single cell analysis, interpretation of calcium data is not quantitative due to fluctuations in basal calcium levels. The sustained elevation of cytosolic calcium concentration during T cell activation leads to nuclear translocation of the transcription factor NFAT, which can occur as early as ~ 1 minute after TCR triggering. After transport, NFAT remains in the nucleus for ~ 20 minutes. Because NFAT can only be found in the nucleus in response to stimulation, monitoring NFAT localization provides a fast and clear readout for T cell activation in a single cell and can be correlated to pMHC:TCR binding data acquired for the same cell.

Figure 4.2A illustrates the quantification of NFAT-mCherry localization in this assay. A stack of epifluorescence images is acquired with an axial slice step size of 3  $\mu\text{m}$  in order to obtain a slice through the middle of the cell. From this slice, we can determine the mean intensity in the cytoplasm and nucleus. When NFAT is fully cytoplasmic, the ratio of these intensities,  $\langle I_{nuc} \rangle / \langle I_{cyt} \rangle$ , is less than 1 (Figure 4.2A, left). When NFAT is fully translocated into the nucleus, the ratio is greater than 1 (Figure 4.2A, right). As proof of concept, we introduced transduced T cells to supported membranes with high or low MCC-MHC densities and monitored the NFAT localization of hundreds of cells interacting with bilayers at each density. The low agonist pMHC density used, 0.03 molecules/ $\mu\text{m}^2$ , is below thresholds for triggering calcium flux,<sup>15</sup> and thus should not stimulate NFAT translocation into the nucleus. In contrast, the high density used, 90 molecules/ $\mu\text{m}^2$ , is well above the thresholds for triggering calcium flux, and therefore should cause NFAT to be shuttled from the cytoplasm into the nucleus. At low density,

most cells have  $\langle I_{nuc} \rangle / \langle I_{cyt} \rangle < 1$ , while at high density,  $\langle I_{nuc} \rangle / \langle I_{cyt} \rangle > 1$  for the majority of cells (Figure 4.2B). These results demonstrate that monitoring NFAT nuclear translocation is a direct method for quantifying T cell activation on the single cell level.

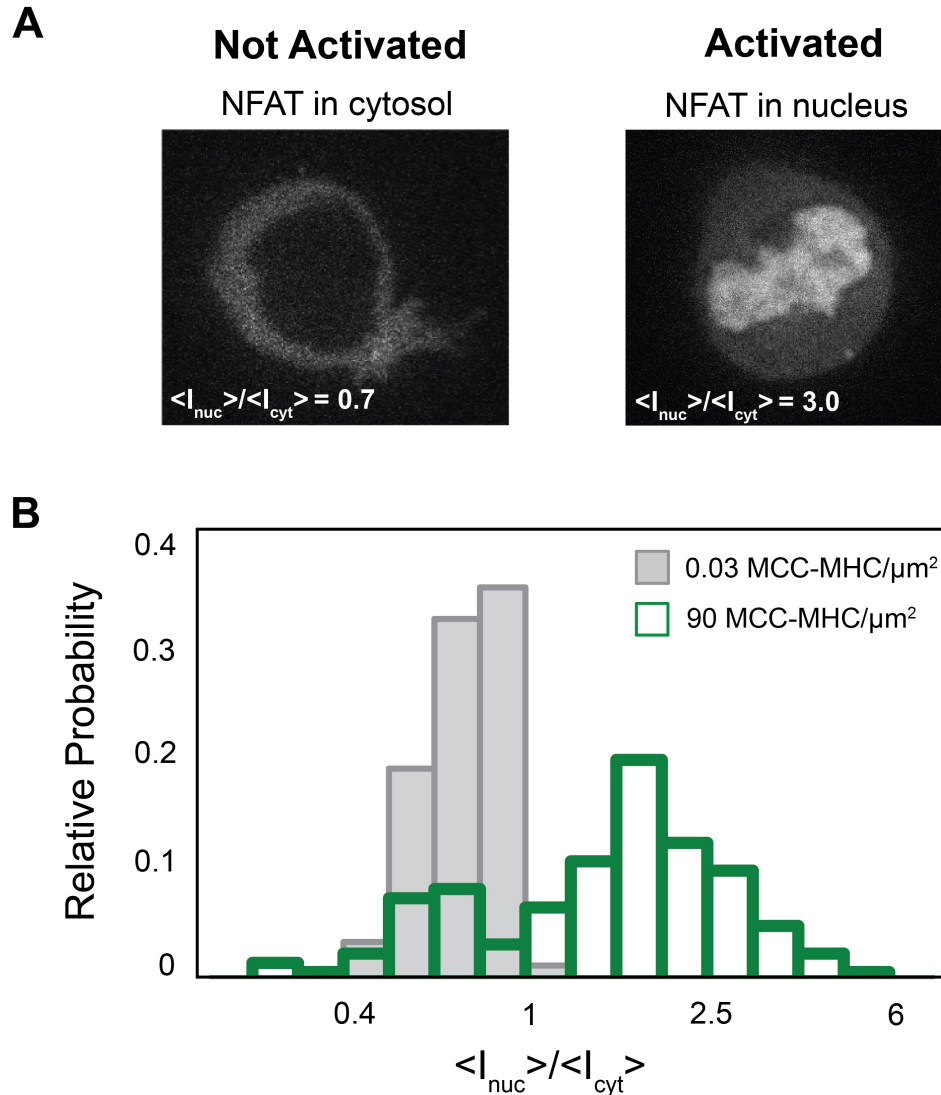


**Figure 4.2: NFAT nuclear translocation is a digital readout of T cell activation.** (A) NFAT is in the cytosol when T cells are not activated (left) and is in the nucleus when T cells are activated (right). The fluorescence intensity ratio between the nucleus and cytoplasm,  $\langle I_{nuc} \rangle / \langle I_{cyt} \rangle$ , is less than one for nonactivated cells and greater than one for activated cells. (B) At low agonist pMHC densities (gray), the majority of cells do not activate, with  $\langle I_{nuc} \rangle / \langle I_{cyt} \rangle < 1$ . At high agonist pMHC densities (green), the majority of cells activate, with  $\langle I_{nuc} \rangle / \langle I_{cyt} \rangle > 1$ .

### Section 4.2.3: Simultaneous observation of pMHC:TCR binding and cellular activation in living T cells

In order to simultaneously detect pMHC:TCR interactions and NFAT localization in a single cell, we devised the imaging scheme illustrated in Figure 4.3. Bound Atto488-pMHC is detected using TIRF microscopy and a 500 ms exposure time. A sequence of images is recorded using a 10 s time lapse. In between the acquisition of each frame in the TIRF time lapse, a stack of epifluorescence images of NFAT-mCherry is recorded. The two imaging methods are alternated until NFAT has fully translocated into the nucleus.

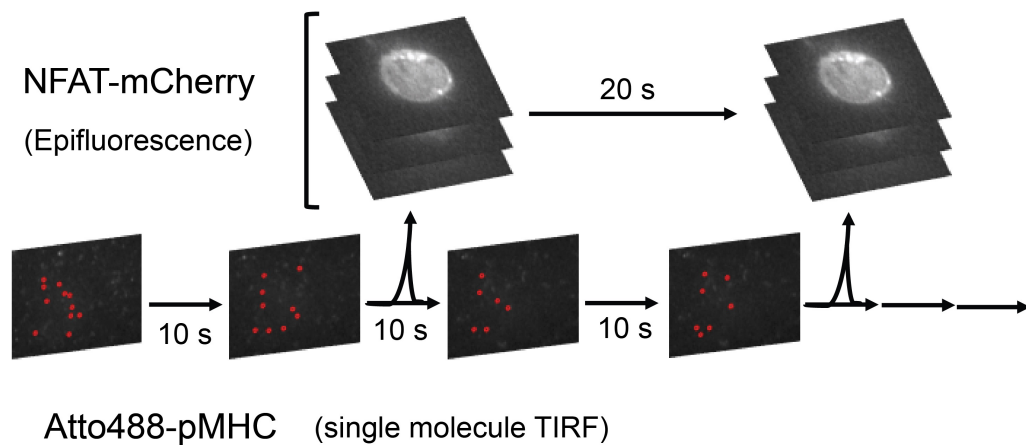


**Figure 4.3: Simultaneous detection of pMHC:TCR binding and NFAT translocation.** Schematic of the imaging technique used to simultaneously observe single molecule pMHC:TCR binding events and NFAT nuclear translocation in living T cells. An imaging sequence of bound Atto488-pMHC is recorded using TIRF microscopy (10 s time lapse, 500 ms exposure time). Between frames, a stack of epifluorescence images of NFAT-mCherry is recorded. The process is repeated until full nuclear translocation is detected.

### Section 4.3: Quantification of pMHC:TCR binding events leading to cellular activation

In order to measure all of the pMHC:TCR binding interactions leading to activation of a single T cell, we simultaneously monitored bound pMHC and NFAT subcellular localization in individual cells using the previously described technique. We measured two binding parameters, total number of cumulative binding events and the cumulative dwell time, the sum of the dwell times of all pMHC:TCR complexes. Figure 4.4 shows these parameters plotted over time leading up until time zero, the first epifluorescence

imaging frame in which NFAT is detected in the nucleus. Figure 4.4A illustrates that there is a wide distribution of total number of binding events required for activation when cells are stimulated with either MCC or T102S. For MCC, the distribution ranges from ~ 30 to ~ 80 binding events, while the range is between ~ 40 and ~ 160 binding events for T102S. This data suggests that T cells require at least 20 TCR binding events for cellular activation as measured by NFAT nuclear translocation. We also observe a wide range of cumulative dwell times leading to activation (Figure 4.4B). The distributions are very similar for stimulation with MCC or T102S and there is a clear threshold of ~ 500 s of cumulative dwell time required for NFAT shuttling to the nucleus.

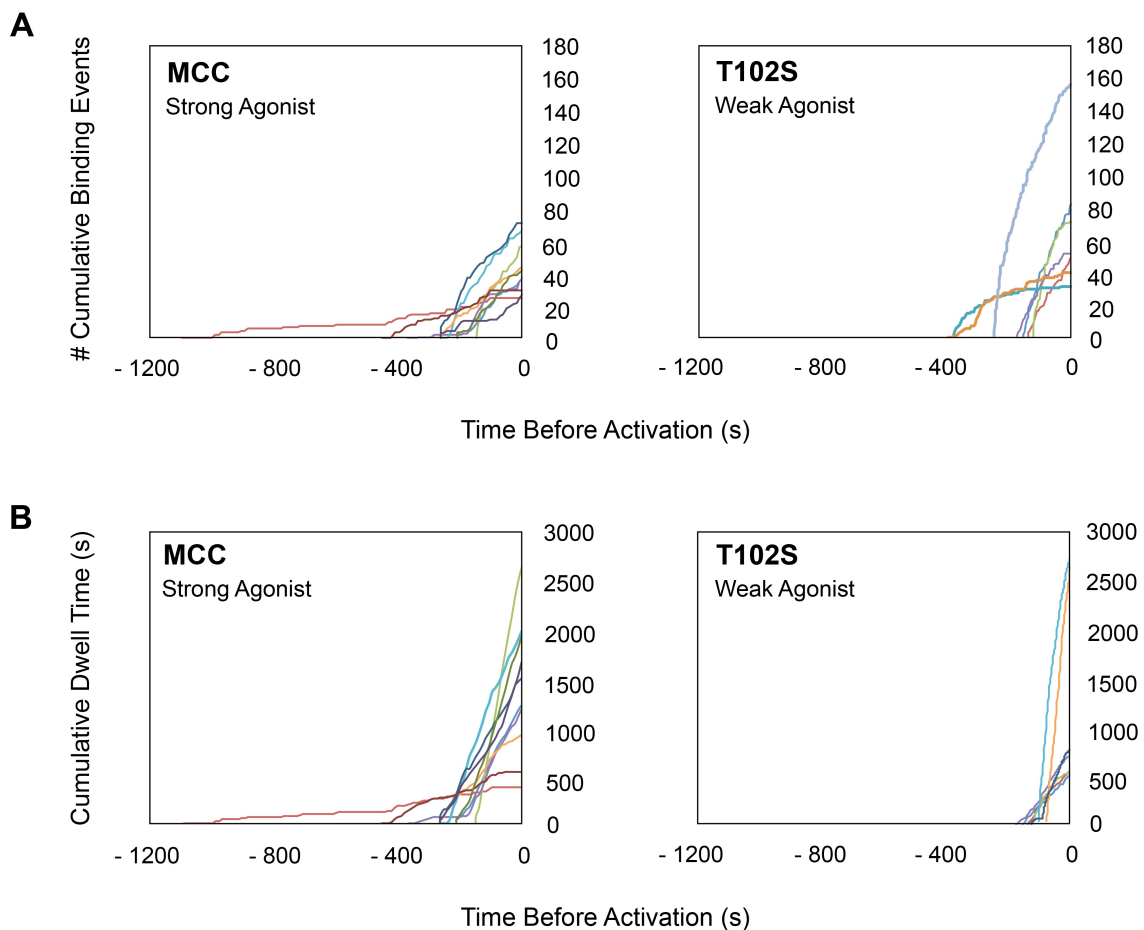


**Figure 4.4: Binding thresholds are required for cellular activation. (A)** The plots show the total number of cumulative pMHC:TCR binding events over time until NFAT is detected in the nucleus. T cells require at least 20 pMHC:TCR complexes for cellular activation. **(B)** The plots show the cumulative pMHC:TCR dwell time for all complexes formed leading to NFAT nuclear translocation. T cells accumulate at least 500 s of dwell time before translocating NFAT.

## **Section 4.4: Discussion and conclusions**

We have constructed a novel system for simultaneously observing single molecule receptor:ligand binding events and downstream cellular activation in a single living T cell. Using this system, we have successfully tracked all of the pMHC:TCR molecular interactions from the time a cell first contacts the supported membrane up until NFAT nuclear translocation is detected. This study is the first report in which every single binding event leading to T cell activation in an individual cell is recorded. Our results show that there is a clear threshold cumulative number of binding events and cumulative dwell time required for NFAT nuclear localization.

These results are consistent with two different previously proposed models of T cell receptor triggering. The first model, the kinetic proofreading model, is based on a minimum lifetime of the pMHC:TCR bond required for the TCR to trigger. This model assumes that the TCR needs to remain bound to a pMHC for it to become fully activated via several steps of modifications.<sup>3</sup> The second model, the TCR occupancy model, proposes that the extent of T cell activation is proportional to the number of TCRs bound by ligand.<sup>16, 17</sup> Because we measure the dwell time of every single pMHC:TCR interaction in an individual cell and report a cumulative dwell time and cumulative number of binding events required for activation, our results incorporate both of these models. Additionally, we demonstrate the heterogeneous distribution of binding events and their associated kinetics within a single cell and across a population of cells.

We investigated the cumulative number of binding events and dwell times leading to NFAT nuclear translocation for TCRs stimulated by strong and weak agonist-MHC molecules. Interestingly, there is no major difference between the thresholds required for cellular activation, suggesting some other mechanism underlying the differences in T cell response.<sup>8, 9</sup> In order to further investigate the effect of peptide potency on the TCR occupancy and cumulative bond lifetimes needed to induce T cell signaling, we are currently examining TCR triggering by the coagonist null peptide ER60 and the strong agonist variant of MCC, K5.<sup>18</sup>

## **Section 4.5: Materials and methods**

### **Section 4.5.1: DNA, protein, and T cell preparation**

Bi-hexahistidine-tagged major histocompatibility complex (MHC) class II I-E<sup>k</sup> protein and decahistidine-tagged ICAM1 were produced and purified as previously described.<sup>10</sup> AND CD4<sup>+</sup> T cells<sup>19</sup> were harvested and cultured essentially as previously described.<sup>20, 21</sup>

The pMSCV-NFAT1<sub>(1-460)</sub>-mCherry plasmid contains a fusion of mCherry with a

truncated murine NFAT1 (NFATc2) gene that lacks most of the DNA-binding domain but incorporates the regulatory domain, which governs nucleocytoplasmic shuttling in NFAT. A pMSCV-NFAT1<sub>(1-460)</sub>-GFP plasmid was a gift of Dr. Thorsten Mempel (Harvard Medical School) and was used to generate the mCherry plasmid using standard cloning procedures.<sup>7</sup> T cells were transduced with NFAT-mCherry using retroviruses harvested from the Platinum Eco packaging cell line.<sup>22</sup> Retroviral transduction with the undiluted pMSCV-NFAT-mCherry supernatants was performed by spin infection on days 3 and 4 after the initial splenocyte harvest. NFAT-mCherry positive cells were sorted using fluorescence-activated cell sorting (FACS) according to viability and mCherry expression. The entire NFAT-mCherry-positive population was used for imaging.

### **Section 4.5.2: Peptide purification and labeling**

Using the basic sequence of moth cytochrome c (amino acids 88–103) and previously described variants,<sup>8, 9</sup> the following peptides were synthesized by David King at the HHMI Mass Spectrometry Laboratory at UC Berkeley and/or commercially (Elim Biopharmaceuticals, Hayward, CA): MCC (ANERADLIAYLKQATK), MCC(C) (ANERADLIAYLKQATKGGSC), T102S (ANERADLIAYLKQASK), T102S(C) (ANERADLIAYLKQASKGGSC). For fluorophore labeling, cysteine-containing peptides were dissolved in a small amount of phosphate buffer and mixed in a 1:2 molar ratio with lyophilized Atto488 (Atto-Tec GmbH, Siegen, Germany) and labeled using maleimide-thiol chemistry. The peptides were then incubated at room temperature for at least 1 hr and purified on a C18 reverse phase column (Grace–Vydac, Deerfield, IL) and H<sub>2</sub>O:acetonitrile gradient using AKTA explorer 100 FPLC system (Amersham Pharmacia Biotech, Piscataway, NJ). Peptide identity was confirmed after purification using mass spectrometry.

### **Section 4.5.3: Imaging chamber and supported lipid bilayer preparation**

Small unilamellar vesicles (SUVs) were formed by tip sonication of a solution composed of 98 mol % 1,2-dioleoyl-sn-glycero-3-phosphocholine (DOPC) and 2 mol % 1,2-dioleoyl-sn-glycero-3-[(N-(5-amino-1-carboxypentyl) iminodiacetic acid) succinyl] (nickel salt) (Ni-NTA-DOGS) (Avanti Polar Lipids, Alabaster, AL) in Milli-Q water (EMD Millipore, Billerica, MA). Tip sonication was preferred to vesicle extrusion due to the introduction of significant levels of fluorescent impurities into the SUVs during extrusion. Prior to experiments, #2 40 mm diameter round coverslips were ultrasonicated for 30 min in 50:50 isopropyl alcohol:water, rinsed thoroughly in Milli-Q water (EMD Millipore, Billerica, MA), etched for 5 min in piranha solution (3:1 sulfuric acid:hydrogen peroxide), and again rinsed thoroughly in Milli-Q water. Bilayers were formed in FCS2 Closed Chamber Systems (flow cells; Biopetechs, Butler, PA), as described in Chapter 2. 48 hr prior to experiments, murine MHC was loaded with peptide (MCC) at 37 °C in a buffer composed of 1% wt/vol bovine serum albumin in phosphate

buffered saline and brought to pH 4.5 with citric acid. Unbound peptide was separated from peptide loaded MHC (pMHC) using 10k molecular weight cutoff Vivaspin centrifugal concentrators (GE Healthcare, Little Chalfont, UK). pMHC and ICAM-1 were diluted with imaging buffer, introduced into the flow cells, and incubated for 35 min followed by a rinse with imaging buffer. Cells were resuspended in imaging buffer and added to the bilayer. Experiments were performed at 37 °C.

#### **Section 4.5.4: Microscopy**

TIRF experiments were performed on a motorized inverted microscope (Nikon Eclipse Ti-E; Technical Instruments, Burlingame, CA) equipped with a motorized Epi/TIRF illuminator, motorized Intensilight mercury lamp (Nikon C-HGFIE), Perfect Focus system, and a motorized stage (Applied Scientific Instrumentation MS-2000, Eugene, OR). A laser launch with a 488 nm (Coherent OBIS, Santa Clara, CA) diode laser was controlled by an OBIS Scientific Remote (Coherent Inc., Santa Clara, CA) and aligned into a fiber launch custom built by Solamere Technology Group, Inc. (Salt Lake City, UT). Laser powers measured at the sample were 0.6 mW for 250 ms exposures and 6 mW for 30 ms exposures. A dichroic beamsplitter (z488/647rpc; Chroma Technology Corp., Bellows Falls, VT) reflected the laser light through the objective lens (Nikon 1.49 NA TIRF; Technical Instruments, Burlingame, CA) and fluorescence images were recorded using an EM-CCD (iXon 897DU; Andor Inc., South Windsor, CT) after passing through a laser-blocking filter (Z488/647M; Chroma Technology Corp., Bellows Falls, VT). Exposure times, multidimensional acquisitions, and time-lapse periods for all experiments were set using Micro-Manager.<sup>23</sup> A TTL signal from the appropriate laser triggered the camera exposure.

Epifluorescence microscopy was performed on a motorized inverted microscope (Nikon Eclipse Ti-E/B, Technical Instruments, Burlingame, CA) equipped with a Nikon 100× Apo TIRF 1.49 NA objective lens, motorized Epi/TIRF illuminator, motorized Intensilight mercury lamp, Perfect Focus system, and a motorized stage (ASI MS-2000, Eugene, OR). All images are collected using a 521 × 521 pixel electron-multiplying charge-coupled device camera (Andor iXon Ultra 897, Technical Instruments, Burlingame, CA). Excitation filters used for Epi illuminations were ET470/40x and ET545/30x. Dichroics were 2 mm thick and mounted in metal cubes to preserve optical flatness: ZT488/647rpc, ZT405/488/561rpc. For epifluorescence images of NFAT translocation, axial slice step size was 3 μm and extended 10 μm above the coverslip, and time lapses are collected at the interval of 50 s.

#### **Section 4.5.5: Data analysis**

Analysis of single pMHC:TCR complexes was performed as previously described.<sup>11</sup> Single molecule diffraction-limited spots were detected in raw .tif image stacks of pMHC

labeled with Atto488 by filtering for both size and intensity and linked into tracks using published particle detection and tracking algorithms<sup>24</sup> adapted for MATLAB (The Mathworks; Natick, MA) by Daniel Blair and Eric Dufresne (<http://physics.georgetown.edu/matlab/>; accessed 16 August 2012). Size and intensity thresholds were first determined by eye using a test data set and then applied uniformly to all data collected with the same exposure time and incident laser intensities. Single molecules were identified by step photobleaching detected in an automated way using a Bayesian change point detection algorithm.<sup>25</sup>

To measure the nuclear translocation of NFAT-mCherry, confocal images of T cells were acquired at 4  $\mu\text{m}$  above the coverslip. For each pMHC density, 40-100 cells were imaged at 10-30 minutes after cell injection. All NFAT-GFP images are analyzed using ImageJ. For each cell, the cytosol and nucleus were identified and masked off as different regions, and the average intensities of the two regions were measured and the ratio  $\langle I_{\text{nuc}} \rangle / \langle I_{\text{cyt}} \rangle$  was calculated. All images with the masked regions were inspected visually. When NFAT is fully cytoplasmic, the ratio is less than 1. When NFAT is fully translocated into the nucleus, the ratio is greater than 1.

## Section 4.6: Chapter 4 references

1. Weiss, A.; Littman, D. R., Signal transduction by lymphocyte antigen receptors. *Cell* **1994**, *76*, 263-274.
2. Valitutti, S.; Dessing, M.; Aktories, K.; Gallati, H.; Lanzavecchia, A., Sustained signaling leading to T cell activation results from prolonged T cell receptor occupancy. Role of T cell actin cytoskeleton. *The Journal of Experimental Medicine* **1995**, *181*, 577-584.
3. McKeithan, T. W., Kinetic proofreading in T-cell receptor signal transduction. *Proceedings of the National Academy of Science* **1995**, *92* (11), 5042-6.
4. Rabinowitz, J. D.; Beeson, C.; Lyons, D. S.; Davis, M. M.; McConnell, H. M., Kinetic discrimination in T-cell activation. *Proceedings of the National Academy of Science* **1996**, *93*, 1401-1405.
5. van der Merwe, P. A.; Dushek, O., Mechanisms for T cell receptor triggering. *Nature Reviews Immunology* **2011**, *11*, 47-55.
6. Macian, F., NFAT proteins: key regulators of T-cell development and function. *Nature Reviews Immunology* **2005**, *5* (6), 472-484.

7. Marangoni, F.; Murooka, T. T.; Manzo, T.; Kim, E. Y.; Carrizosa, E.; Elpek, N. M.; Mempel, T. R., The transcription factor NFAT exhibits signal memory during serial T cell interactions with antigen-presenting cells. *Immunity* **2013**, *38*, 237-249.
8. Matsui, K.; Boniface, J. J.; Steffner, P.; Reay, P. A.; Davis, M. M., Kinetics of T-cell receptor binding to peptide/I-Ek complexes: Correlation of the dissociation rate with T-cell responsiveness. *Proceedings of the National Academy of Science* **1994**, *91*, 12862-12866.
9. Rogers, P. R.; Grey, H. M.; Croft, M., Modulation of naive CD4 T cell activation with altered peptide ligands: The nature of the peptide and presentation in the context of costimulation are critical for a sustained response. *The Journal of Immunology* **1998**, *160* (8), 3698-3704.
10. Nye, J. A.; Groves, J. T., Kinetic control of histidine-tagged protein surface density on supported lipid bilayers. *Langmuir* **2008**, *24* (8), 4145-4149.
11. O'Donoghue, G. P.; Pielak, R. M.; Smoligovets, A. A.; Lin, J. J.; Groves, J. T., Direct single molecule measurement of TCR triggering by agonist pMHC in living primary T cells. *Elife* **2013**, *2*, e00778.
12. Khoruts, A.; Mondino, A.; Pape, K. A.; Reiner, S. L.; Jenkins, M. K., A natural immunological adjuvant enhances T cell clonal expansion through a CD28-dependent, interleukin (IL)-2-independent mechanism. *The Journal of Experimental Medicine* **1998**, *187* (2), 225-236.
13. Sojka, D. K.; Bruniquel, D.; Schwartz, R. H.; Singh, N. J., IL-2 secretion by CD4<sup>+</sup> T cells in vivo is rapid, transient, and influenced by TCR-specific competition. *The Journal of Immunology* **2004**, *172* (10), 6136-6143.
14. Huse, M.; Klein, L. O.; Girvin, A. T.; Faraj, J. M.; Li, Q.-J.; Kuhns, M. S.; Davis, M. M., Spatial and temporal dynamics of T cell receptor signaling with a photoactivatable agonist. *Immunity* **2007**, *1* (27), 76-88.
15. Manz, B. N.; Jackson, B. L.; Petit, R. S.; Dustin, M. L.; Groves, J. T., T-cell triggering thresholds are modulated by the number of antigen within individual T-cell receptor clusters. *Proceedings of the National Academy of Science* **2011**, *108* (22), 9089-9094.
16. Matis, L. A.; Glimcher, L. H.; Paul, W. E.; Schwartz, R. H., Magnitude of response of histocompatibility-restricted T-cell clones is a function of the product of the concentrations of antigen and Ia molecules. *Proceedings of the National Academy of Science* **1983**, *80*, 6019-6023.

17. Zarnitsyna, V.; Zhu, C., T cell triggering: insights from 2D kinetics analysis of molecular interactions. *Physical Biology* **2012**, *9* (045005).
18. Krogsgaard, M.; Li, Q.; Sumen, C.; Huppa, J. B.; Huse, M.; Davis, M. M., Agonist/endogenous peptide–MHC heterodimers drive T cell activation and sensitivity. *Nature* **2005**, *434*, 238-243.
19. Kaye, J.; Hsu, M.-L.; Sauron, M.-E.; Jameson, S. C.; Gascoigne, N. R.; Hedrick, S. M., Selective development of CD4+ T cells in transgenic mice expressing a class II MHC-restricted antigen receptor *Nature* **1989**, *341*, 746-749.
20. Smith, A. W.; Smoligovets, A. A.; Groves, J. T., Patterned two-photon photoactivation illuminates spatial reorganization in live cells. *Journal of Physical Chemistry A* **2011**, *115*, 3867-3875.
21. Smoligovets, A. A.; Smith, A. A.; Wu, H.-J.; Petit, R. S.; Groves, J. T., Characterization of dynamic actin associations with T-cell receptor microclusters in primary T cells. *Journal of Cell Science* **2012**, *125*, 735-742.
22. Morita, S.; Kojima, T.; Kitamura, T., Plat-E: an efficient and stable system for transient packaging of retroviruses. *Gene Therapy* **2000**, *7* (12), 1063-1066.
23. Stuurman, N.; Edelstein, A. D.; Amodaj, N.; Hoover, K. H.; Vale, R. D., Computer control of microscopes using Micro-Manager. **2010**, 1-22.
24. Crocker, J. C.; Grier, D. G., Methods of digital video microscopy for colloidal studies. **1996**, *179*, 298-310.
25. Ensign, D. L.; Pande, V. S., Bayesian detection of intensity changes in single molecule and molecular dynamics trajectories. **2009**, *114* (1), 280-292.